frontiers | Frontiers in Earth Science

TYPE Original Research
PUBLISHED 30 September 2024
DOI 10.3389/feart.2024.1407400

OPEN ACCESS

EDITED BY
Idoia Rosales,
CN Instituto Geológico y Minero de España (IGME, CSIC), Spain

REVIEWED BY
Pablo Suarez-Gonzalez,
Complutense University of Madrid, Spain
Irene Gomez-Perez,
Independent Practitioner, Muscat, Oman

*CORRESPONDENCE
Xiaohong Liu,
liuxiaohong_swpu@163.com
Mingyou Feng,
fmyswpu@163.com

RECEIVED 26 March 2024
ACCEPTED 03 September 2024
PUBLISHED 30 September 2024

CITATION
Li Y, Zhang B, Zhou G, Tang R, Long H, Li C, Chen X, Chen D, Liu X, Zhang C and Feng M (2024) Lithofacies and diagenetic controls on thrombolitic dolomite reservoir development from the Precambrian Dengying Formation in the central Sichuan Basin, SW China. *Front. Earth Sci.* 12:1407400. doi: 10.3389/feart.2024.1407400

Lithofacies and diagenetic controls on thrombolitic dolomite reservoir development from the Precambrian Dengying Formation in the central Sichuan Basin, SW China

Yong Li[1], Benjian Zhang[1], Gang Zhou[1], Ruifeng Tang[2], Hongyu Long[1], Chenglong Li[1], Xi Chen[1], Di Chen[1], Xiaohong Liu[3]*, Chao Zhang[3] and Mingyou Feng[3]*

[1]Exploration and Development Research Institute, PetroChina Southwest Oil and Gasfield Company, Chengdu, China, [2]Exploration Division of PetroChina Southwest Oil and Gasfield Company, Chengdu, China, [3]School of Geoscience and Technology, Southwest Petroleum University, Chengdu, China

Microbialite reservoirs are of great importance in oil and gas exploration. However, there is still a lack of comprehensive studies on the formation mechanisms of thrombolitic reservoirs, a specific type of microbialite. This research focuses on the oldest thrombolitic dolomite reservoir located within the Precambrian Dengying Formation in the central Sichuan Basin, southwestern China. A multi-disciplinary approach was employed to characterize different thrombolite facies and elucidate the formation mechanism of thrombolitic dolomite reservoirs and their controlling factors, involving core observation, thin-section analysis, cathodoluminescence, scanning electron microscope (SEM) microscopy, elemental analysis using LA-ICP-MS, and carbon and oxygen stable isotope analysis. Based on variations in texture, four types of thrombolite were identified: 1) distinct clotted thrombolite, 2) diffuse and regular clotted thrombolite, 3) diffuse and irregular clotted thrombolite, and 4) composite clotted thrombolite. Notably, the diffuse clotted thrombolitic dolomite is the prevalent lithology in the reservoir. Through modification by meteoric water, organic acid fluids, and hydrothermal fluids, a reservoir with dominant porosity in the form of primary growth-framework pores, dissolution pores, and vugs was formed. This resulted in the development of two high-quality reservoir intervals within the Second Member and at the top of the Fourth Member of the Dengying Formation. The growth-framework porosity of the thrombolites, epigenetic karstification, and tectonic fracturing were mainly conducive to reservoir development. However, various types of cementation have reduced porosity and connectivity within the reservoir. Overall, this study is a valuable example of the methodology required to understand meso- and microstructures

of deep-buried thrombolitic dolomite reservoirs, including their heterogeneities and diagenesis, as the original structures influence diagenesis.

KEYWORDS

thrombolite, dolomite reservoir, diagenesis, Precambrian Dengying Formation, central Sichuan Basin

1 Introduction

Microbialites are lithified structures formed through the accretion and preservation of microbial films and mats facilitated by sediment trapping, binding, and mineral precipitation by benthic microbial communities (Burne and Moore, 1987; Riding, 2000; Suarez-Gonzalez et al., 2019a). These microbialites can be categorized into four types based on their morphological and structural characteristics: thrombolite, stromatolite, leiolite, and dendrolite (Riding, 2000; Grey and Awramik, 2020). Throughout geological history, microbialites have thrived in various periods, particularly during the Neoproterozoic Era, and have been documented in regions such as the Great Basin, northeastern Gulf of Mexico, Sichuan Basin and Tarim Basin in China, Oman Basin, and Zagros Basin (Mancini et al., 2004; 2006; Harwood and Sumner, 2012; Grotzinger and Al-Rawahi, 2014; Harwood Theisen and Sumner, 2016; Song et al., 2017; Jafarian et al., 2018; Suarez-Gonzalez et al., 2019b; Chen et al., 2023). Some exploration of oil and gas resources has mainly focused on microbialite units, such as the Ara Group in the Oman Basin and the Precambrian Dengying Formation in the Sichuan Basin, China, where stromatolites and thrombolites are the predominant reservoir rocks in the shallow-water carbonate platform facies (Grotzinger and Al-Rawahi, 2014; Yang et al., 2022). Understanding the development and distribution of Neoproterozoic microbialites is essential for gaining insight into contemporary geological processes and ecosystems (Altermann and Corcoran, 2002; Suarez-Gonzalez et al., 2019b). Furthermore, these investigations carry substantial implications for exploring oil and gas in ancient carbonate rocks at deep (≥4.5 km) to ultra-deep depths (≥6 km) (Wen et al., 2023).

Thrombolites, a typical type of microbialite, are differentiated from other types of microbialite, such as stromatolites and dendrolites, based on their internal clotted and patchy fabric (Aitken, 1967; Kennard and James, 1986; Shapiro, 2000). Thrombolites may display some degree of lamination due to periodic sedimentation rather than deliberate trapping and binding of sediments to form the well-defined, regular lamination observed in stromatolites as a result of binding by microbial communities (Arp et al., 1998; Riding, 2000). Thrombolites usually coexist with stromatolites in shallow intertidal to subtidal environments. Thrombolites could form in relatively deeper and lower energy hydrodynamic environments and gradually transition to stromatolites toward shallow zones (Dupraz and Visscher, 2005; Mancini et al., 2006; Suarez-Gonzalez et al., 2019a). The distinct fabric of thrombolites and the depositional settings in which they develop make them valuable indicators of ancient environmental conditions and microbial ecosystems (Bosak et al., 2013; Tang et al., 2013).

Identifying and interpreting thrombolite variations requires systematic observation and definition of their internally clotted or patchy fabric (Harwood Theisen and Sumner, 2016). However, the scale diversity of the thrombolite structures and the modification of the depositional fabrics by post-depositional processes have complicated the terminology used in describing thrombolites over time (Aitken, 1967). Various terms have been used, such as thrombolite (Aitken, 1967), fenestrae (Pratt, 1982), mesoclots (Kennard and James, 1986), clotted macrostructures (Riding, 1991), thromboids (Kennard, 1994), and microclots (Shapiro, 2000). To address this, it is more reasonable and effective to describe macrostructures on the decimeter-to-meter scales as thrombolites, mesoscopic structures on the millimeter-to-decimeter scales as mesoclots, and microscopic structures on the micrometer-to-sub-millimeter scales as microclots (Grey and Awramik, 2020). Furthermore, previous research on microbialites in Montana, Oman, and the Sichuan Basin has often treated microbialites as a whole, focusing on the types of reservoir rocks, their characteristics, and modifications induced by diagenesis and tectonic events (Katz et al., 2006; Grotzinger and Al-Rawahi, 2014; Shen et al., 2019). These studies have focused mainly on stromatolites, providing valuable insights into their sedimentary environments, fabric characteristics, controlling factors, and mechanisms governing reservoir formation (Moore and Burne, 1994; Zhu et al., 2021). The limited research specifically addressing thrombolites and their unique characteristics makes it necessary to conduct more research on these distinct types of microbialites, particularly regarding their depositional conditions, fabric characteristics, and factors controlling thrombolitic reservoir development.

In recent years, remarkable progress has been made in oil and gas exploration in the late Precambrian Dengying Formation located in the central Sichuan Basin, southwestern China. These advancements have revealed the potential of deep to ultra-deep-buried microbial dolomite reservoirs as promising hydrocarbon reservoirs (Wen et al., 2023). The development of the primary reservoir is controlled by the sedimentary environment, while the genesis mechanism of deep to ultra-deep-buried thrombolitic dolomite reservoirs is particularly complex due to multiple stages of modification by diagenetic fluids and tectonic events (Feng et al., 2017). However, limited research has focused on thrombolitic dolomite reservoirs, particularly regarding the meso-micro scale differences of these reservoirs. Furthermore, the genesis and evolution of thrombolitic dolomite reservoirs and the modification mechanisms that create high-quality reservoirs remain relatively unexplored.

This paper focuses on the deep to ultra-deep-buried thrombolitic dolomite reservoir found within the Precambrian Dengying Formation in the central Sichuan Basin. Detailed investigations have been conducted into its petrology, reservoir characteristics, and diagenesis. The main goals of the study are 1) to elucidate key characteristics of the thrombolitic dolomite reservoirs, 2) to decipher the formation mechanisms of the reservoir, and 3) to

provide a crucial workflow to characterize microbialite reservoirs in deep to ultra-deep-buried carbonate rocks.

2 Geological setting

The Sichuan Basin, located in southwestern China within the western region of the Yangtze Craton, is an intracontinental basin that was filled by multiple sedimentary packages, separated by unconformities, deposited on the Archean-early Proterozoic crystalline basement (Liu et al., 2021). The basin can be divided into six tectonic units, with the research area located in the central folded-faulted belt (CFFB) (Figure 1A). During the Precambrian and Cambrian, the northwestern region of the Yangtze Craton (NYC) experienced rifting due to the extension of the Rodinia supercontinent, resulting in the formation of the Deyang-Anyue intracratonic rift, which was a synsedimentary rift controlled by the regional Xingkai extensional tectonic event (Figure 1A) (Scotese, 2009; Wen et al., 2022; Yang et al., 2022). The NYC region then experienced tectonic uplift and stratigraphic erosion due to the episodic Tongwan tectonic event (TW-I, TW-II) during the late Precambrian, leading to the formation of multistage unconformity surfaces at the top of the Second and Fourth Members of the Dengying Formation (Song et al., 2017). Subsequently, from the Late Silurian to the Early Permian, tectonic compression and uplift associated with the Qilian and Yunnan tectonic events caused the erosion of early Paleozoic strata, forming the western uplifted region in the Sichuan Basin (Wan, 2012). During the Late Permian to Early Triassic, an extensional tectonic setting prevailed in the area, marked by the Dongwu tectonic event, the eruption of the Emeishan basalts, and regional tectonic uplift, which resulted in emersion and short-term erosion of the central Sichuan Basin and formed a large number of fractures (F_I). During the Middle and Late Triassic, the basin remained stable and experienced subsidence, followed by a compressional setting during the Late Jurassic to Early Cretaceous due to tectonic inversion, leading to the southeastward migration of the western paleohigh. During the Middle and Late Mesozoic, multidirectional compression along the basin margins caused the depression of the basin and the development of a series of foreland basins in the Cretaceous. Since the Cenozoic, the central Sichuan Basin has experienced significant uplift and formed later fractures (F_{II}), influenced by the effects of the collision between the Indian and Asian plates (Jiang et al., 2014; Liu et al., 2021).

The Dengying Formation in the central Sichuan Basin is generally buried at depths exceeding 5,000 m, with a thickness ranging from 650 m to 1,000 m. It is unconformably overlain by black siliceous and carbonaceous shales and muddy siltstones of the Lower Cambrian Maidiping or Qiongzhusi formations, which have a thickness of 300 m–1,000 m. It is underlain by the sandstones and dolomitic mudstones of the Doushantuo Formation, which has a thickness of 10 m–500 m (Figure 1B) (Song et al., 2017). The Dengying Formation can be divided into four members from bottom to top: Dengying First, Second, Third, and Fourth Members. The thickness of the Dengying Formation progressively diminishes as it approaches the northeastern margin of the rift, where the Dengying Third and Fourth Members are missing, due either to non-deposition or because they are entirely eroded, while the Second Member is partially eroded and shows an unconformable contact with the overlying Lower Cambrian Qiongzhusi or Maidiping formations (Figure 1) (Zhang et al., 2005). In the study area, the Dengying First Member consists mainly of dark gray microbial-poor dolomicrites and lamellar dolomites with a thickness of 24 m–230 m. The Second Member is mainly composed of massive dark gray thrombolitic dolomites, stromatolitic dolomites, and dolograinstones, ranging in thickness from 100 m to 800 m. The Third Member consists of dark gray muddy dolomites, sandy dolomites, and minor dolomicrites, with a thickness of 0 m–70 m. The Dengying Fourth Member is dominated by light gray to dark gray stromatolitic dolomites, thrombolitic dolomites, and dolograinstones with a thickness of 0 m–400 m (Figure 1B) (Wen et al., 2023).

Two third-order transgression-regression cycles were recorded in the Precambrian Dengying Formation (Jin et al., 2020) (Figure 1B). The First and Third Members of the Dengying Formation were deposited during transgressive stages, while the Second and Fourth Members were deposited during regression (Jin et al., 2020). The Dengying Second and Fourth Members developed carbonate platforms and platform margins with high volumes of microbial mound and shoal facies (Figure 1B) (Wen et al., 2023). Stromatolites and thrombolites are commonly found in microbial mounds (Song et al., 2017). Furthermore, hydrocarbon charging occurred from the Middle Ordovician to the Late Silurian and from the Middle Permian to the Middle Triassic, resulting in the formation of two stages of paleo-reservoirs. Subsequently, these hydrocarbons experienced oxidation or cracking, leading to the formation of bitumen due to tectonic uplift in the late Paleozoic and rapid subsidence from the early to middle Triassic, respectively (Yuan et al., 2014; Yang et al., 2023).

3 Samples and methods

In this study, we conducted core description, sampling, and analysis of 11 wells (434.69 m of cores in total) drilled in the Precambrian Dengying Formation in the central Sichuan Basin. These wells covered the main thrombolitic reservoir intervals of the Dengying Second and Fourth Members (Figure 1B). Additionally, we conducted an outcrop description of the thrombolitic dolomite in the Gucheng area on the northern margin of the basin (Figure 1A). To systematically analyze the petrological characteristics, reservoir characteristics, and diagenetic paragenesis, we used standard thin-section observation (41 samples) under a petrographic microscope, thin-section analysis by cathodoluminescence microscopy (CL, 29 samples), and helium porosity and air-permeability analysis of core plugs (59 samples). To differentiate calcite and dolomite, thin sections were dyed using a mixture of alizarin red S and potassium ferricyanide. Freshly cracked surfaces of thrombolitic dolomites (15 samples) were selected for micro-morphological analysis and examined using a scanning electron microscope (SEM). All analyses were carried out at the National Experimental Teaching Center for Oil and Gas Geology and Exploration at Southwest Petroleum University, using the following instruments: Olympus BX53 microscope, CL8200 MK5 cathodoluminescence microscope, CMS™-300 Core Measuring System, and FEI Quanta 650 FEG scanning electron microscope, respectively.

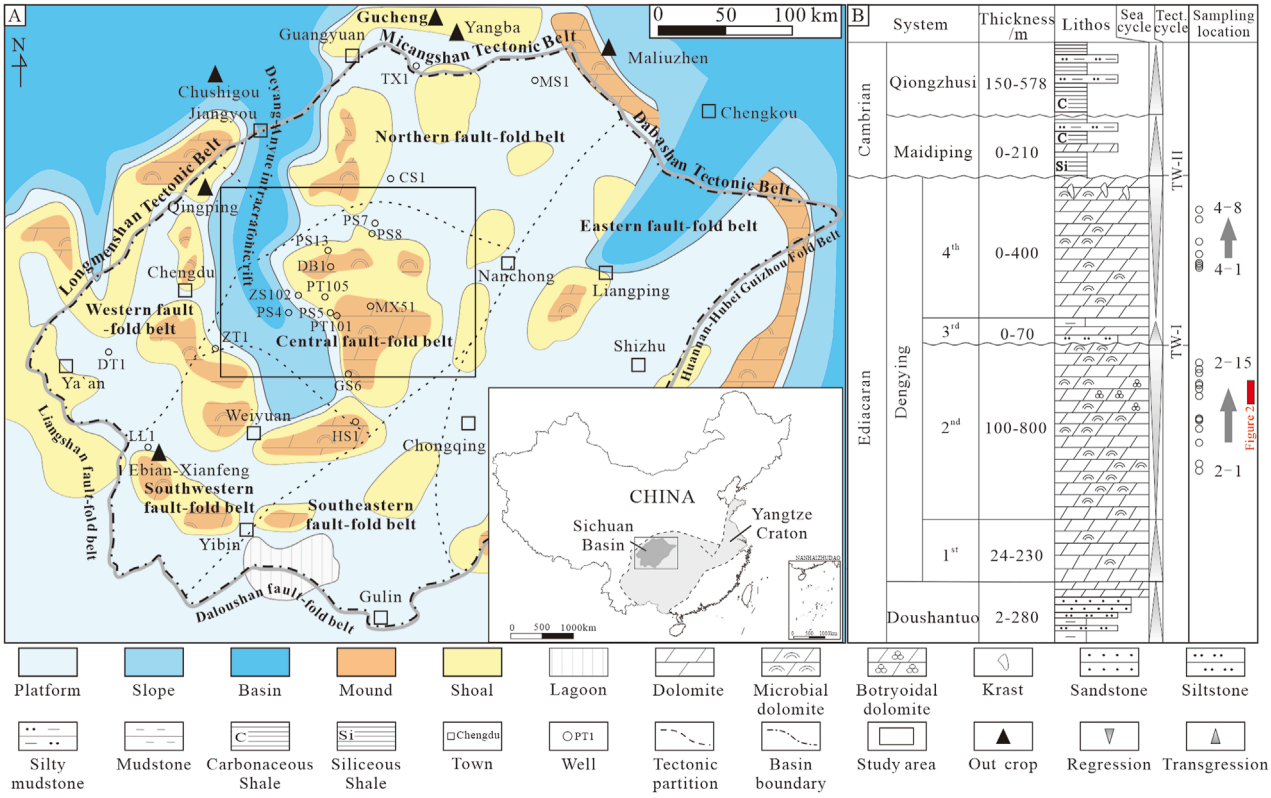

FIGURE 1
Precambrian paleogeographic and tectonic sketch **(A)** and stratigraphic column of the Precambrian Dengying Formation in the central Sichuan Basin **(B)**, modified from Wen et al. (2022). TW-I = Episode I of the Tongwan uplift tectonic event, TW-II = Episode II of the Tongwan uplift tectonic event. Microbial mounds and shoals correspond to microbial buildups and dolograinstone deposits, respectively.

Trace and rare earth element (REE) analyses were conducted on different types of dolomite cement and matrix in 23 polished thin sections. These analyses were performed using laser ablation inductively coupled plasma mass spectrometry (LA-ICP-MS) at Sichuan Chuangyuan Weipu Analytical Technology Co. Ltd. The LA-ICP-MS system utilized a resolution LR 193 nm ArF excimer laser ablation system coupled with a Thermo iCAP TQ mass spectrometer. Laser ablation was carried out with a spot size of 67 μm, a repetition rate of 10 Hz, and a fluence of 3 J/cm^2. The principal calibration standard used was NIST 614, following the methods described by May et al. (2000) and Thompson and Taylor (2008). Data reduction was performed using IOLITE software.

Stable isotopic ($\delta^{18}O$, $\delta^{13}C$) analyses were conducted on 56 polished thin sections of thrombolitic matrix and cement dolomites. The analyses were carried out at the Southwest Petroleum University employing the standard carbonate reaction method. Laser ablation sampling was employed to collect CO_2 from the carbonate rocks for subsequent mass spectrometry analysis. The samples underwent the phosphoric acid bath method at 90°C to generate CO_2, which was then examined using an Elementar IsoPrime GC5 mass spectrometer. Standard isobaric corrections were adopted. All stable isotope data were converted to permil (‰) relative to Vienna Pee Dee Belemnite (V-PDB) and corrected by fractionation factors provided by Fairchild and Spiro (1987). The precision of the $\delta^{18}O$ and $\delta^{13}C$ ratios is better than ±0.1‰.

4 Results

4.1 Macroscopic and microscopic examination

Outcrop and core observations reveal that the thickness of the thrombolites in the Dengying Formation varies from the centimeter to the decimeter scale, with some thrombolite complexes extending to the meter scale, forming mounds. The outcrop study has revealed a cyclic arrangement of the depositional facies associated with the thrombolites (Figures 3A, B). The sedimentary cycle, from bottom to top, consists of light gray to gray dolomicrite (microbial mound base or cap), gray to dark gray thrombolitic dolomite, and stromatolitic dolomite (microbial mound core) (Figures 2, 3A). Core observations of the Dengying Formation show that thrombolitic mounds predominantly consist of a gray to dark gray dolomicrite matrix and light gray dolomite cement, with thrombolites often exhibiting mesoscopic laminations with a thickness of 1 mm–10 mm (Figures 3C–F).

Under the microscope, the dolomicrite matrix consists of gray to dark gray microclots. Based on variations in the microstructure

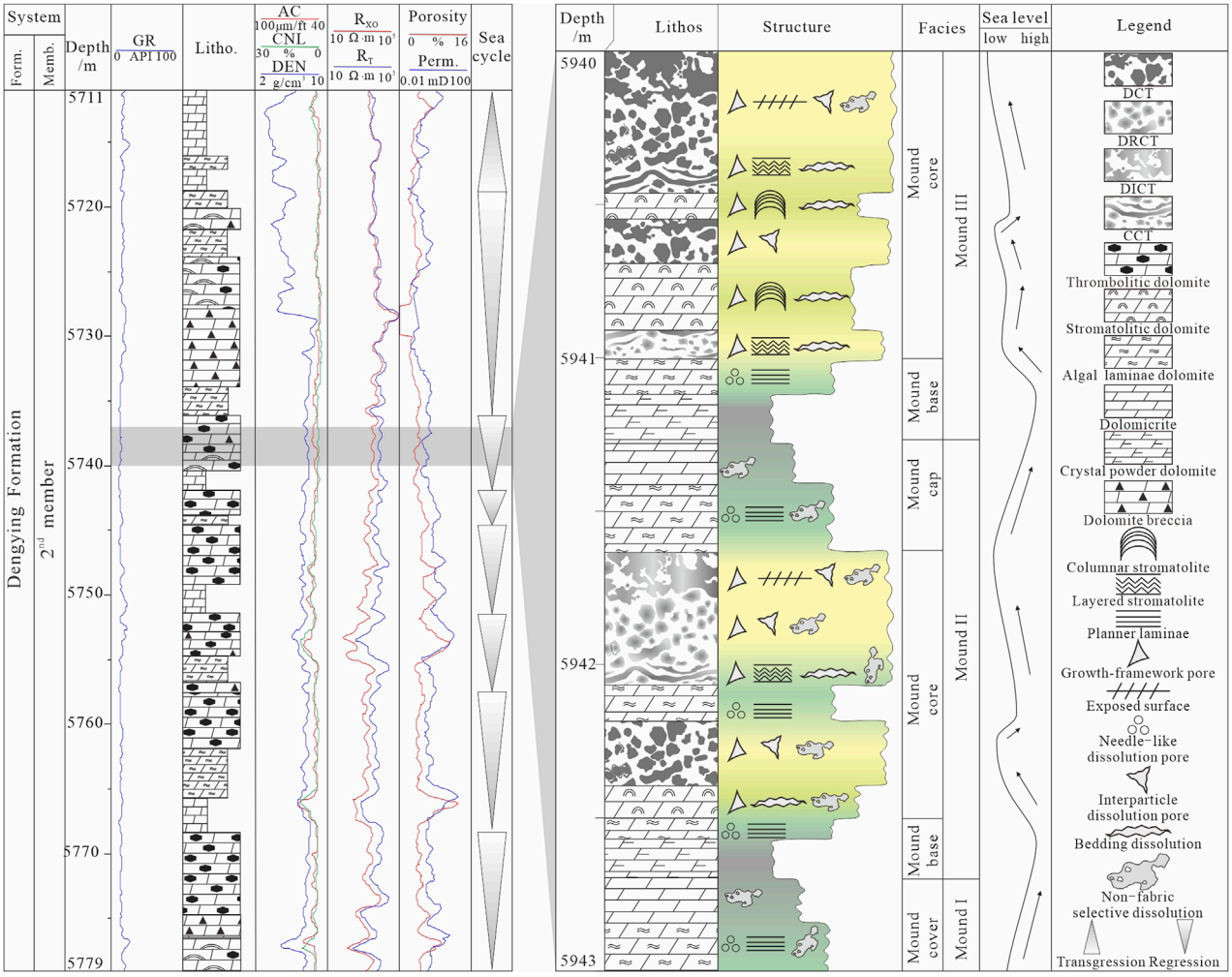

FIGURE 2
Dengying Second Member core data and description from well PT101. Note the vertical distribution of different thrombolites at the meter scale. The relative locations of the cored sections have been labeled in Figure 1B. Form, formation; Memb., member; GR, gamma ray; AC, acoustic logs; CNL, compensated neutron logs; DEN, density logs; RT, log curve of uninvaded zone resistivity; RXO, log curve of flushed zone resistivity; Perm, permeability.

of the dolomicrite matrix (Harwood and Sumner, 2012), four types of thrombolites can be identified: distinct clotted thrombolite (DCT), diffuse and regular clotted thrombolite (DRCT), diffuse and irregular clotted thrombolite (DICT), and composite clotted thrombolite (CCT) (Figure 4).

The different types of thrombolites are often mixed or transitional with each other or with other microbialites. Specifically, the DCT displays continuous corrugated mesoclotted laminations in shades of light gray to gray on the well cores, with lamination thicknesses ranging from 1 mm to 10 mm. Light gray cements can be observed between the gray laminations (Figure 3C). Microscopic analysis reveals the occurrence of well-defined dolomicrite microclots of dark gray to black colors that are typically spherical, sub-spherical, or flower-shaped, with a relatively uniform size ranging from 30 μm to 300 μm. The microclots are often densely packed, forming a network-like structure. Within the microclots, authigenic quartz crystals measuring 15–20 μm and pyrite with diameters of 10 –20 μm can be observed (Figure 4A). In contrast, the DRCT exhibits gray to dark gray sub-continuous corrugated mesoclotted laminations with thicknesses less than 5 mm on the well cores. Light gray dolomite cements can be seen between the laminations (Figure 3D). Under microscopic examination, it is characterized by light gray to gray dolomicrite microclots with diffuse transitional boundaries. These microclots are predominantly spherical or sub-spherical, with variable particle sizes ranging from 40 μm to 500 μm and occasionally reaching 1 mm. They are often mixed and transitional with dark gray microclots, forming sub-spherical, mound-like mesoclots with particle sizes ranging from 200 μm to 800 μm. Some of these microclots are in close contact. A few authigenic quartz and pyrite crystals can also be seen in the microclots (Figure 4B).

The DICT is characterized by a discontinuous appearance, with dark gray diffuse to patchy laminated or clustered structures measuring less than 2 mm. Additionally, light gray non-laminated diffuse mesoclots are present but can be difficult to identify on the well cores (Figure 3E). Microscopic analysis reveals that

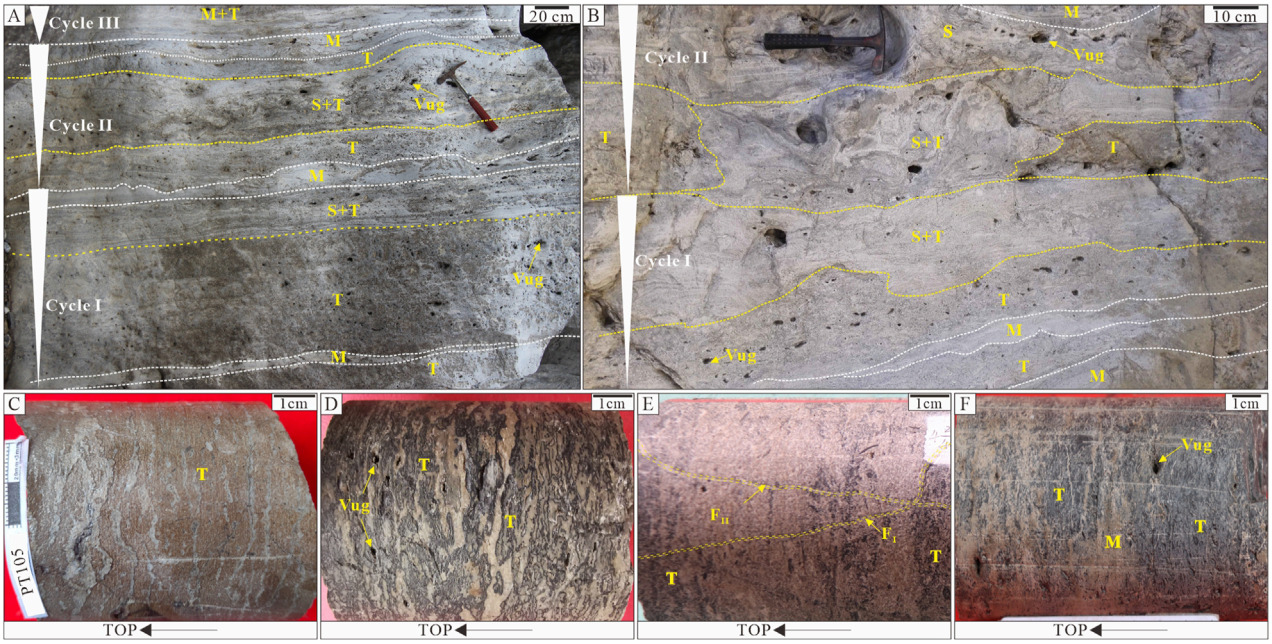

FIGURE 3
Macroscopic and mesoscopic characteristics of thrombolitic dolomite for the Precambrian Dengying Formation from the Gucheng outcrop and cores in the central Sichuan Basin. **(A, B)** Dolomicrites, thrombolites, and stromatolites developed in vertical sequences (cycles I, II, and III) of the Second Member at the Gucheng outcrop, located on the northern margin of the Sichuan Basin; **(C)** distinct clotted thrombolite (DCT) with continuous corrugated laminations, 2-6, core, PT105, 5,941.22 m, Second Member; **(D)** diffuse and regular clotted thrombolite (DRCT) with sub-continuous corrugated laminations and vugs, 2-3, core, ZS102, 6,046.69 m, Second Member; **(E)** diffuse and irregular clotted thrombolite (DICT) with discontinuous, less than 2-mm dark gray diffuse patchy or clustered laminae, and fractures (F_I, F_{II}), 2-2, core, PS4, 6,207.70 m, Second Member; **(F)** composite clotted thrombolite (CCT) showing a mixture of dark gray domal, discontinuous corrugated and laminated mesoclots, and vugs, 4-2, core, DB1, 6,407.58 m, Fourth Member. T, thrombolite; S, stromatolite; M, dolomicrite; S+T, mixed layer of stromatolites and thrombolites; F_I, earlier filled fracture; F_{II}, later fracture unfilled; the black arrows point to the top of the formation in Figures **(C–F)**.

DICT comprises microclots, which are agglomerates of light gray to gray dolomicrite. These microclots exhibit irregular shapes and a wide range of sizes, varying from 150 μm to 1,200 μm. The microclots have diffuse overgrowth of boundaries and are mixed with dark gray to gray-black microclots (Figures 4C, D). Finally, in the well-core description, CCT occurs as a mixture of dark gray domal, discontinuous corrugated, and laminated mesoclots. These mesoclots typically range in size from 2 mm to 5 mm and exhibit mixed fabrics of distinct, diffused, or laminated microclots. However, identifying CCT on core samples can be difficult (Figure 3F). Microscopic observations demonstrate the presence of intergrowths or irregular transitions between microclots and corrugated microclots (Figures 4E–H). Some microclots exhibit branching patterns, with both diffuse and well-distinguished boundaries, as well as diffuse and irregular microclots (Figures 4E, F, H). Certain CCT consists of dark gray laminated mesoclots, interbedded with light gray microbial-bearing dolomicrite, with net or diffuse laminated boundaries and light gray laminations (Figures 4F–H). Moreover, some discontinuous diffuse microclotted laminations evolve upwards into diffuse domal microclots and are integrated into the dolomicrite matrix (Figure 4L). Most of these assemblages are sub-millimeter in size and exhibit significant vertical variations.

Overall, the four types of thrombolite mentioned above, both in the outcrop and in the cores, exhibit continuous corrugated laminations, sub-continuous corrugated laminations, discontinuous laminations, or are massive (Figures 3C–F). The variations in color, shape, size, and composition can be clearly observed under the microscope. The main differences between DCT and diffuse thrombolite, DRCT, and DICT are the net boundaries with light gray cement or diffuse transitions between both (Figures 4E–H). Compared to DRCT, DICT displays irregular shapes and variations in scale (Figures 4F–H). CCT is commonly found mixed with microclotted laminations, and its microclots exhibit diverse types that can be identified as individual microclots from the three types of thrombolite mentioned above (Figures 4I–L).

4.2 Diagenesis

A systematic study of the thrombolitic dolomite reservoir revealed the products of different diagenetic processes, including dolomitization, dissolution, physical and chemical compaction, recrystallization, and cementation. The cross-cutting relationships of different diagenetic events were identified to create a paragenetic sequence.

4.2.1 Precursor aragonite and/or calcite cementation

The different pore types present in all types of thrombolites typically exhibit a similar mineral infilling sequence, and four

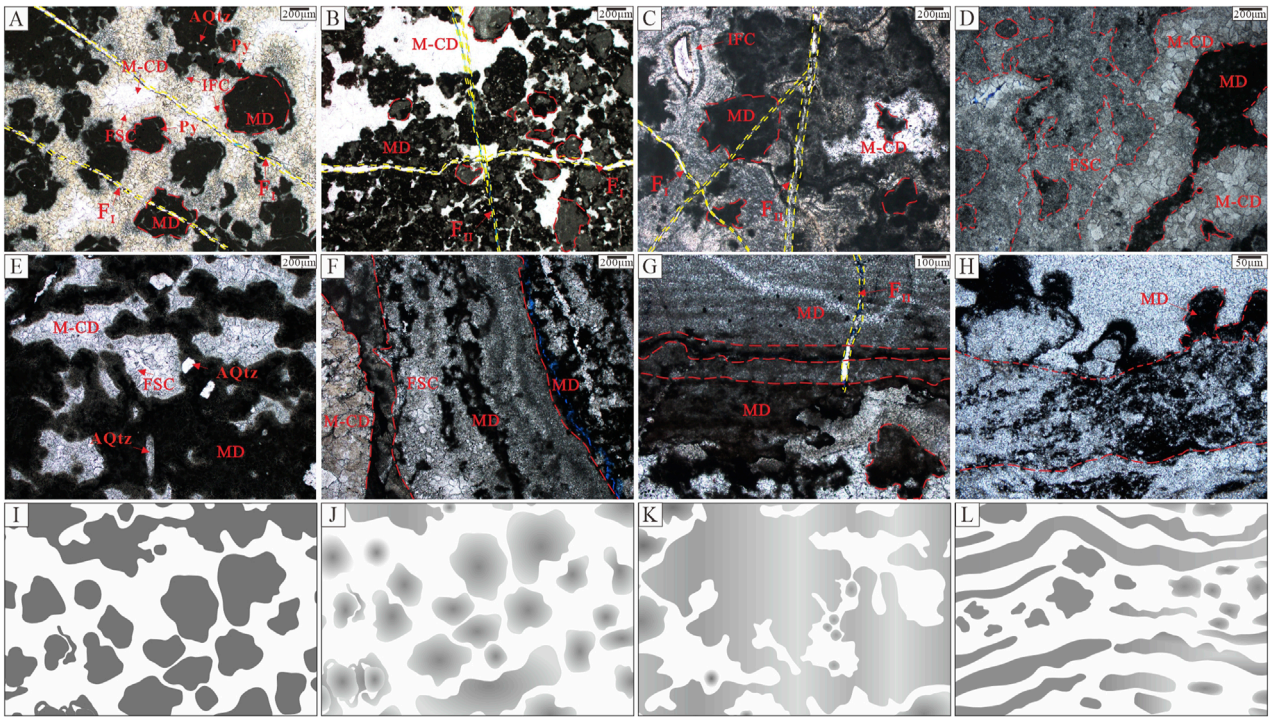

FIGURE 4
Microscopic characteristics of thrombolitic dolomite for the Precambrian Dengying Formation. **(A)** DCT with isopachous fibrous cement and M-CD cementing in the growth-framework pores and fractures (F_I), photomicrograph of Figure 3C; **(B)** DRCT with diffuse and regular microclots and fractures (F_I, F_{II}), photomicrograph of Figure 3D; **(C)** DICT with diffuse and irregular microclots and fractures (F_I, F_{II}), photomicrograph of Figure 3E; **(D)** DICT with FSC and M-CD cementing in the growth-framework pores and vugs, photomicrograph of Figure 3F; **(E)** CCT with diffuse and irregular clotted branches and cementation by the FSC and M-CD in growth-framework pores. Authigenic quartz (AQtz) occurs in the microclots, 2-12, PS5, 5,682.99 m, Second Member; **(F)** CCT with diffuse and irregular microclots, microclotted lamination, and growth-framework pores cemented by FSC and M-CD, 2-12, PS5, 5,682.99 m, Second Member; **(G)** CCT with distinct and irregular clots growing downward and upward from laminations, PS5, 5,682.99 m, Second Member; **(H)** CCT with distinct and branching clots growing upward and in sharp contact with the matrix dolomite (MD), 2-13, GS6, 5,388.11 m, Second Member. **(I–L)** Sketch of DCT, DRCT, DICT, and CCT, respectively. All the above photomicrographs A-H were taken under plane-polarized light. MD, thrombolitic matrix dolomite; IFC, isopachous fibrous cement; FSC, fine crystalline spar cement; M-CD, medium to coarse crystalline dolomite cement; SD, saddle dolomite cement; F_I, earlier filled fracture; F_{II}, later fracture unfilled or partially filled with quartz.

consecutive stages of cementation can be identified: isopachous fibrous cement (IFC), fine crystalline spar cement (FSC), medium to coarse crystalline dolomite cement (M-CD) and saddle dolomite cement (SD) (Figures 5A–C). The latter two cements are primary dolomite precipitations, which will be described in detail in the following sections. Isopachous fibrous cement consists of gray, fibrous, or needle-like crystals that cover the edges of microclots, forming an isopachous cement coat with a thickness ranging from 80 μm to 200 μm. This cement is dull to blotchy under CL (Figures 5A, B). Fine crystalline spar cement is composed of light gray, subhedral crystals that often grow in continuity with the isopachous fibrous cement or fill dissolution pores (Figures 5A, B) or vugs. The crystal sizes range from 50 μm to 80 μm and are bright red under CL (Figure 5C). The isopachous fibrous and fine crystalline spar cements are mineralogically dolomite in the present day, although they most likely originally precipitated as high-Mg calcite or aragonite (IFC) and low-Mg calcite (FSC), respectively.

4.2.2 Dolomitization

Dolomitized thrombolites and cements are recorded in the cores and outcrops. The thrombolites from the Dengying Formation in the central Sichuan Basin are composed of dark gray dolomicrite. SEM analysis shows the occurrence of spherical particle dolomite and dolomitic microbial extracellular polymers (EPs) attached to the surface of the dolomite crystals within the microclots (Figure 5G). The energy spectrum analysis results (EDS) indicated that the EPs consisted of Ca, Mg, C, and O elements (Figure 5I). Additionally, the isopachous fibrous and fine crystalline spar cements are considered to be replaced by dolomite (Figures 4A, B).

4.2.3 Dissolution

Dissolution resulted in the formation of a variety of irregular pores and vugs, ranging in size from millimeter to centimeter scales. These pores and vugs formed through various processes, including the intra- and inter-particle dissolution of microclots. Occasionally, dissolution breccias are seen (Figures 5C, F). Three types of dissolution processes can be identified: 1) Epigenetic dissolution mainly involves the thrombolitic growth-framework pores. The dissolution of the thrombolite fabrics resulted in isolated or elongated pores following the bedding planes and vugs ranging in size from millimeters to centimeters (Figures 3A–D, F). These pores and vugs have relatively smooth edges and are subsequently filled with fine crystalline spar cements and medium to coarse crystalline dolomite cements. 2) Burial dissolution mainly expands

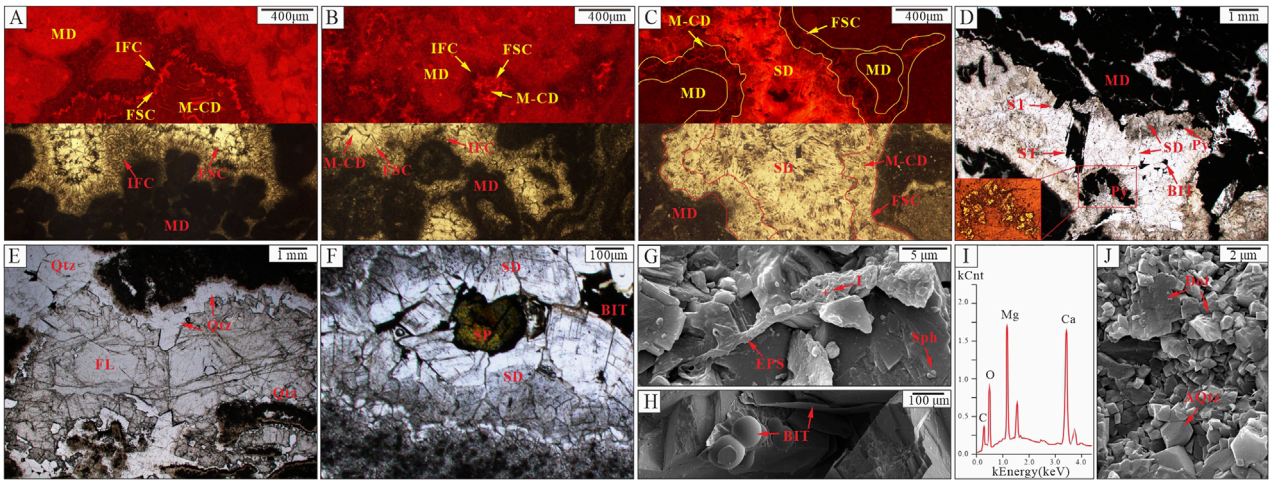

FIGURE 5
CL, microscopic, and SEM characteristics of multistage cements and microbial fabrics in thrombolitic dolomite for the Precambrian Dengying Formation. **(A)** DCT with isopachous fibrous cement and FSC and M-CD cementing in the growth-framework pores, 2-8, ZS102, 6,055.92 m, Second Member, CL and plane-polarized light; **(B)** DICT with isopachous fibrous cement, FSC and M-CD cementing in the growth-framework pores, 2-10, PS2, 5,712.06 m, Fourth Member, CL and plane-polarized light; **(C)** DICT with FSC, M-CD, and SD cementing in a meteoric dissolution vug, 4-2, DB1, 6,407.58 m, Fourth Member, CL and plane-polarized light; **(D)** DCT with SD, bitumen (BIT) and pyrite (Py) filling in a hydrothermal dissolution vug; note the occurrence of a stylolite, 4-2, DB1 6,407.57 m, Fourth Member. Plane-polarized light and the lower left figure of pyrite display an enlarged view of the red portion in Figure D using polarized reflected light; **(E)** DCT with quartz (Qtz) and fluorite (FL) filling in a hydrothermal dissolution vug, 4-5, PS13, 6,711.53 m, Fourth Member, plane-polarized light; **(F)** DRCT with saddle dolomite cement (SD), sphalerite (SP) and bitumen (BIT) filling in a hydrothermal dissolution pore, 2-1, PS4, 6,215.84 m, Second Member, plane-polarized light; **(G)** dolomitic microbial extracellular polymers (EPs) and spherulites (Sph) in the diffuse microclot, 2-1, PS4, 6,215.84 m, Second Member, SEM; **(H)** bubble, film of bitumen (BIT) filling in an intercrystalline pore of a diffuse microclot, 2-1, PS4, 6,215.84 m, Second Member, SEM; **(I)** EDS result showing the major-element composition of the dolomitic EPs in Figure G; **(J)** dolomicrite crystals of 0.5 μm–4 μm in size, which are in interlocking contact, and authigenic euhedral quartz (AQtz) within the distinct microclot, 2-5, PT105, 5,942.45 m, Second Member, SEM. MD, thrombolitic matrix dolomite; IFC, isopachous fibrous cement; FSC, fine crystalline spar cement; M-CD, medium-to-coarse crystalline dolomite cement; SD, saddle dolomite cement.

growth-framework pores and intercrystalline pores and dissolves microclots to form new irregular dissolution pores and vugs. These irregular pores are non-fabric selective and are commonly filled with bitumen (Figures 6B, C). Dissolution-enlarged fractures also occur during this stage and are typically connected to the pores and vugs, contributing to their enlargement and connectivity. Under a petrographic microscope and SEM, bitumen can be observed as encrustations, amorphous masses, bubbles, or films (Figures 5D, F). 3) Burial hydrothermal dissolution typically results in the formation of non-fabric selective irregular pores and vugs. The size of these pores can vary from millimeters to centimeters. Saddle dolomite and quartz commonly fill these pores, with occasional fluorite and sphalerite (Figures 5D–F).

4.2.4 Physical and chemical compaction

The thrombolitic dolomite underwent intense physical and chemical compaction during burial. The compaction is mainly manifested by the deformation of sedimentary structures and the formation of concavo-convex or sutured contacts and stylolites (Figures 5D, 6B).

4.2.5 Recrystallization

Recrystallization is often manifested as changes in crystal morphology and size, with little change in mineral composition. The thrombolitic dolomites exhibit limited evidence of recrystallization. The dark gray microclots show minimal signs of recrystallization textures for the dolomicrite crystals, which range in size from 0.5 μm to 4 μm with interlocking dolomicrite contacts under the SEM (Figures 4A–H, 5J). However, the adjacent light gray to gray non-thrombolitic dolomite matrix displays dolomite crystals ranging in size from 8 μm to 25 μm with interlocking dolomicrite contacts (Figures 4F–H). Authigenic quartz is present as euhedral crystals with blotchy surfaces within the dark gray microclots (Figures 4A, E, 5J).

4.2.6 Late dolomite cementation

Medium to coarse dolomite cement is characterized by clean, euhedral crystals filling pores after the fine crystalline spar cement. These crystals have sizes ranging from 100 μm to 2 mm and are dark red under CL (Figures 5A–C). Saddle dolomite cement consists of non-planar subhedral crystals with dirty surfaces, exhibiting sweeping extinction under an orthogonal polarizer (Figures 5C, D). These crystals range in size from 100 μm to 2 mm and fill pores after medium to coarse crystalline dolomite cement or are precipitated within fractures and between tectonic breccias (Figures 5C, D).

4.3 Porosity and permeability of thrombolitic dolomites

Various types of open porosity are found in the thrombolitic dolomite reservoirs within the Dengying Formation in the

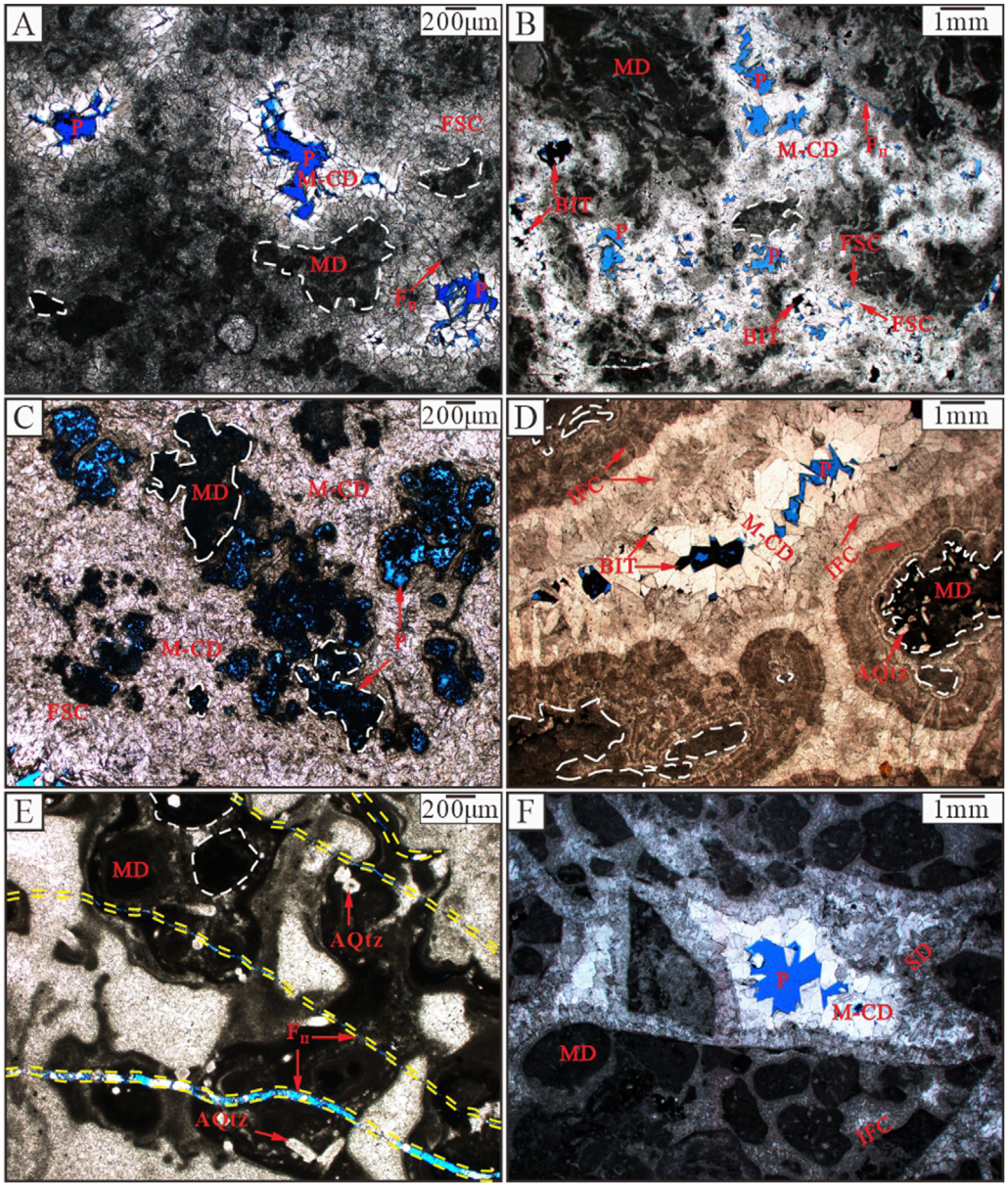

FIGURE 6
Porosity types of the thrombolitic dolomite reservoirs of the Precambrian Dengying Formation in the central Sichuan Basin. **(A)** DICT, exhibiting dissolution pores cemented by FSC and M-CD. Partially preserved dissolution pores are highlighted in blue epoxy, 4-7, PS2, 7,780.61 m, Fourth Member; **(B)** CCT with dissolution pores and vugs partially filled by multistage dolomite cements and bitumen. Rarely, M-CD shows irregular dissolution pores (in blue epoxy) probably produced by organic acids, 4-8, PS8, 7,050.89 m, Fourth Member; **(C)** DCT with microclot matrix exhibiting intraparticle dissolution pores. Dolomite and bitumen are present within the growth-framework pores, 2-4, PT101, 5,771.30 m, Second Member; **(D)** DRCT with growth-framework pores filled by a multistage succession of consecutive early to late cements from isopachous fibrous cement to M-CD cement, forming a botryoidal structure. Authigenic quartz (AQtz) is observed within the thrombolite, and remaining pores (in blue epoxy) are partly filled with bitumen, 2-14, PS5, 5,686.98 m, Second Member; **(E)** DRCT with open tectonic fractures partially filled with dolomite. Authigenic quartz (AQtz) is present within the matrix, 2-11, PS5, 5,709.93 m, Second Member; **(F)** DCT with tectonic fractures and breccias sequentially filled with SD and M-CD, preserving residual porosity (in blue epoxy) in the center, 2-15, PS5, 5,669.68 m, Second Member. All the above photomicrographs were taken under plane-polarized light. MD, thrombolitic matrix dolomite; IFC, isopachous fibrous cement; FSC, fine crystalline spar cement; M-CD, medium-to-coarse crystalline dolomite cement; SD, saddle dolomite cement; F_{II}, later fracture unfilled or partially filled with quartz; BIT, bitumen.

central Sichuan Basin. The main types include growth-framework pores, intraparticle dissolution pores within the microclots, as well as occasionally dissolution vugs (>2 mm) and tectonic fractures (Figures 3D, F, 4B). Growth-framework pores are principally found in DICT and CCT dolomites, and these pores are partially filled with fine and medium to coarse crystalline dolomite cements (Figures 4A, B). However, fractures can cut through the DCT dolomites (Figures 4A, 6E). Intraparticle pores are relatively well-developed within the DRCT microclots (Figure 6C). Moreover, there are two stages of tectonic

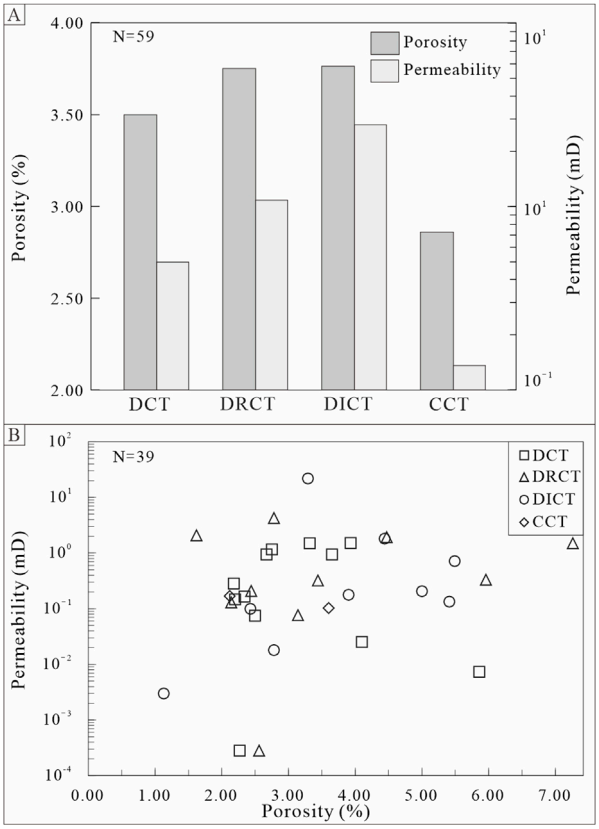

FIGURE 7
Statistical analysis of porosity and permeability measurements in the four types of thrombolitic dolomite reservoirs made on core plugs from the Precambrian Dengying Formation. **(A)** Distribution characteristics of average porosity and permeability of the four types of thrombolitic dolomite reservoirs; **(B)** Porosity versus permeability scatter plot of different thrombolitic dolomite reservoirs for the Precambrian Dengying Formation in the central Sichuan Basin.

fractures, with earlier fractures being mostly filled with saddle dolomite and medium to coarse crystalline dolomite, while later fractures are unfilled or partially filled with quartz (Figures 3E, 4A–C, G).

The porosity and permeability of the four types of thrombolitic dolomite differ slightly (Figure 7), and they are generally classified as relatively low-porosity and ultra-low-permeability reservoirs. The porosity of DCT ranges from 0.97% to 8.23%, with an average value of 3.50%. The permeability ranges from 0.0003 mD to 1.520 mD, with an average value of 0.4970 mD. The porosity of DRCT ranges from 1.62% to 7.26%, with an average value of 3.75%. The permeability ranges from 0.0003 mD to 4.2600 mD, with an average value of 1.0844 mD. The porosity of DICT ranges from 1.13% to 5.49%, with an average value of 3.76%. The permeability ranges from 0.0030 mD to 21.9841 mD, with an average value of 2.7945 mD. The porosity of CCT ranges from 2.12% to 3.60%, with an average value of 2.86%. The permeability ranges from 0.1026 mD to 0.1690 mD, with an average value of 0.1358 mD.

4.4 Element geochemistry and carbon and oxygen stable isotope data

The trace element analysis aimed to investigate the composition of the thrombolitic dolomite matrix and cements found in the Dengying Formation. The elements studied were Na, K, Fe, Mn, Sr, and Ba. The Mg/Ca and Fe/Mn ratios were also examined (Table 1; Figure 9). The results of comparing the matrix and cements show that the thrombolitic dolomite matrix and isopachous fibrous cement have high contents of Na+K, with mean values of 3,180.88 ppm and 4,540.50 ppm, respectively. Fe and Mn are present in relatively low contents, with the matrix showing mean contents of 310.33 ppm for Fe and 291.96 ppm for Mn. In the isopachous fibrous cement, the mean concentrations of Fe and Mn are 165.06 ppm and 174.08 ppm, respectively. The two have similar mean Fe/Mn ratios of 1. Fine crystalline spar cement has mean Na+K, Fe, and Mn contents of 3,330.44 ppm, 138.24 ppm, and 313.60 ppm, respectively, and a lowest mean Fe/Mn ratio of 0.33. The medium to coarse crystalline dolomite cement has mean Fe and Mn content of 295.90 ppm and 274.22 ppm, respectively. The mean Na+K content is relatively low, at 264.30 ppm, and the mean Fe/Mn ratio is 2.31. The saddle dolomite cement within the fractures exhibits elevated mean Fe and Mn contents of 822.83 ppm and 1858.01 ppm, respectively. The saddle dolomite cement has a high mean Fe/Mn ratio of 2.34 and a low Na+K content below 0.1 ppm. In general, the mean Mg/Ca ratios of matrix and cements differ slightly (ranging from 0.69 to 0.72). In contrast, the mean Ba contents in the cements are less than 10.00 ppm, whereas the matrix has a mean Ba content of 162.79 ppm. Moreover, from the matrix to the saddle dolomite cement, the mean Sr contents gradually decrease from 68.26 ppm to 43.88 ppm with increased burial depth (Table 1; Figure 9).

The REE analysis was performed using the REE+Y partitioning method, with standardization by post-Archean Australian Shale (PAAS) (McLennan, 1989) (Table 2; Figure 10). The thrombolitic dolomite matrix displayed negative Ce anomalies with a mean Ce/Ce^* of 0.025 and a flat REE pattern (Table 2; Figure 10A). The isopachous fibrous cement exhibited slightly negative Ce anomalies with a mean Ce/Ce^* of 0.005 and low ΣREE (Table 2; Figure 10A). The fine crystalline spar cement was enriched in heavy rare earth elements (HREEs), while the medium to coarse crystalline dolomite cement showed positive Eu anomalies with a mean Eu/Eu^* of 0.082 and enrichment of HREEs (Table 2; Figure 10B). Additionally, the medium to coarse crystalline dolomite cement to saddle dolomite, which filled the vugs, displayed a relatively flat REE pattern (Table 2; Figure 10C). The saddle dolomite cement filling the fractures showed positive Eu anomalies with a mean Eu/Eu^* of 0.309 and enrichment in middle rare earth elements (MREEs) (Table 2; Figure 10D).

The results of the stable carbon and oxygen isotope analysis indicate that the dolomite matrix has $\delta^{13}C$ values ranging from +1.04‰ to +3.38‰, with an average of +2.02‰, while the $\delta^{18}O$ values range between −4.74‰ and −1.45‰, with an average of −3.40‰. In contrast, the isopachous fibrous cement has $\delta^{13}C$ values ranging from +0.70‰ to +3.73‰, with an average of +1.87‰, while the $\delta^{18}O$ values range between −6.91‰ and −2.85‰, with an average of −4.89‰. The fine crystalline spar cement exhibits $\delta^{13}C$ values ranging from +0.76‰ to +2.87‰, with an average of

TABLE 1 Trace element concentrations (ppm) of thrombolitic matrix and different cements determined by LA-ICP-MS for the Precambrian Dengying Formation in the central Sichuan Basin.

Type	Num	Well ID	Form	Depth	Mn	Fe	Na+K	Sr	Ba	Mg/Ca	Fe/Mn
				m	ppm	ppm	ppm	ppm	ppm		
MD	2-1	PS4	2nd	6,215.84	145.65	125.90	3,260.34	53.10	50.84	0.73	0.86
	2-7	PT105	2nd	5,940.00	341.03	537.66	4,194.89	94.84	338.88	0.69	1.58
	4-6	PS7	4th	7,245.68	389.19	267.42	2087.40	56.84	98.64	0.71	0.69
IFC	2-1	PS4	2nd	6,215.84	240.57	396.05	2,271.93	40.67	3.49	0.72	1.65
	2-3	ZS102	2nd	6,146.69	237.33	91.46	5,624.78	62.67	12.45	0.75	0.39
	2-7	PT105	2nd	5,940.00	182.49	126.07	6,980.13	83.57	13.23	0.67	0.69
	4-6	PS7	4th	7,245.68	35.91	46.65	3,285.16	37.18	9.32	0.67	1.30
FSC	2-1	PS4	2nd	6,215.84	90.27	52.10	ND	22.91	ND	0.70	0.58
	2-3	ZS102	2nd	6,146.69	127.07	330.86	3,330.44	59.88	1.41	0.73	0.38
	2-7	PT105	2nd	5,940.00	723.45	31.77	ND	44.88	1.43	0.68	0.04
M-CD	2-1	PS4	2nd	6,215.84	318.18	127.20	358.95	41.17	6.93	0.72	0.40
	2-1	PS4	2nd	6,215.84	78.89	103.85	ND	26.77	0.23	0.73	1.32
	2-1	PS4	2nd	6,215.84	293.81	346.44	ND	28.01	ND	0.73	1.18
	2-1	PS4	2nd	6,215.84	359.15	388.74	288.62	30.99	1.61	0.72	1.08
	2-3	PS4	2nd	6,215.84	460.28	958.05	18.74	20.65	1.83	0.72	2.08
	2-3	ZS102	2nd	6,146.69	94.35	111.72	ND	23.15	ND	0.74	1.18
	4-6	PS7	4th	7,245.68	314.90	35.27	390.87	161.04	20.24	0.69	8.93
SD	2-7	PT105	2nd	5,940.00	1773.75	650.22	ND	45.80	0.86	0.69	2.73
	2-7	PT105	2nd	5,940.00	1942.27	995.43	ND	41.96	ND	0.69	1.95

MD, thrombolitic matrix dolomite; IFC, isopachous fibrous cement; FSC, fine crystalline spar cement; M-CD, medium-to-coarse crystalline dolomite cement; SD, saddle dolomite cement; Second, Second Member of Dengying Formation; Fourth, Fourth Member of Dengying Formation; ND, not detected.

+2.05‰, while the $\delta^{18}O$ values range between −8.87‰ and −6.09‰, with an average of −7.44‰. The medium to coarse crystalline dolomite cement has $\delta^{13}C$ values ranging from +0.90‰ to +3.16‰, with an average of +1.97‰, while the $\delta^{18}O$ values range between −9.65‰ and −5.86‰, and average −7.49‰. Furthermore, the saddle dolomite cement exhibits $\delta^{13}C$ values ranging from −0.00‰ to +2.12‰, with an average of +1.16‰, while the $\delta^{18}O$ values range between −13.2‰ and −8.72‰, with an average of −10.77‰ (Table 3; Figure 8).

5 Discussion

5.1 Thrombolite deposition

The Dengying Formation in the central Sichuan Basin can be divided into two third-order transgressive-regressive cycles, as mentioned above. In addition, outcrop and core observations show that multiple millimeter-centimeter scale shallowing-upward sub-cycles from dolomicrites to thrombolites and/or stromatolites were developed in the middle and upper parts of the Dengying Second and Fourth Members, resulting in the deposition of microbialites (Figures 2, 3A), and coinciding with the maximum regression of the respective third-order cycles. In these shallow sedimentary environments, microbial communities can promote the direct precipitation of carbonate from carbonate-oversaturated marine water (Burne and Moore, 1987; Riding, 2000) and lithification by the calcification of cyanobacteria to form microbialites, such as thrombolites and stromatolites (Harwood and Sumner, 2012). Primary dolomite may also be precipitated in the microbialites because microbial mediation is the only known mechanism that promotes precipitation of primary dolomite at low temperature (Vasconcelos et al., 2005; Yuan et al., 2022). In this study, the macroscopic vertical contact

10.3389/feart.2024.1407400

TABLE 2 Rare earth element concentrations (ppm) of dolomitic thrombolite and thrombolitic matrix and different cements determined by LA-ICP-MS for the Precambrian Dengying Formation in the central Sichuan Basin.

Type	Num	Well ID	Form	Depth	La	Ce	Pr	Nd	Sm	Eu	Gd	Tb	Dy	Y	Ho	Er	Tm	Yb	Lu	ΣREE+Y	Ce/Ce*	Eu/Eu*
				m	ppm	ppm	ppm	ppm	ppm	ppm	ppm	ppm	ppm	ppm	ppm	ppm	ppm	ppm	ppm	ppm		
MD	2-1	PS4	2nd	6,215.84	2.308	2.650	0.514	2.213	0.466	0.099	0.565	0.087	0.664	9.201	0.165	0.522	0.074	0.464	0.061	20.054	0.033	0.092
	2-7	PT105	2nd	5,940.00	1.458	2.355	0.323	1.304	0.243	0.068	0.281	0.034	0.207	1.885	0.038	0.103	0.012	0.071	0.010	8.393	0.030	0.063
	4-6	PS7	4th	7,245.68	0.872	1.006	0.135	0.468	0.111	0.015	0.112	0.017	0.097	0.980	0.024	0.049	0.008	0.034	0.006	3.933	0.013	0.014
IFC	2-1	PS4	2nd	6,215.84	0.849	0.528	0.137	0.610	0.091	0.023	0.162	0.022	0.208	3.421	0.050	0.148	0.018	0.105	0.018	6.390	0.007	0.021
	2-3	ZS102	2nd	6,146.69	0.285	0.458	0.062	0.278	0.055	0.007	0.064	0.008	0.060	0.853	0.015	0.043	0.005	0.021	0.004	2.219	0.006	0.006
	2-7	PT105	2nd	5,940.00	0.240	0.373	0.050	0.188	0.039	0.009	0.022	0.004	0.027	0.305	0.005	0.020	0.001	0.015	0.001	1.299	0.005	0.008
	4-6	PS7	4th	7,245.68	0.079	0.114	0.014	0.038	0.010	0.003	0.006	0.001	0.005	0.088	0.001	0.005	ND	ND	ND	0.365	0.001	0.003
FSC	2-1	PS4	2nd	6,215.84	0.575	1.806	0.382	1.745	0.448	0.103	0.484	0.084	0.608	5.789	0.142	0.433	0.062	0.409	0.057	13.128	0.023	0.095
	2-3	ZS102	2nd	6,146.69	0.134	0.201	0.018	0.061	0.007	0.002	0.011	0.002	0.016	0.437	0.008	0.018	0.003	0.019	0.002	0.939	0.003	0.002
	2-7	PT105	2nd	5,940.00	1.063	2.618	0.411	1.691	0.429	0.112	0.509	0.077	0.534	4.127	0.115	0.305	0.040	0.226	0.031	12.288	0.033	0.104
M-CD	2-1	PS4	2nd	6,215.84	0.457	1.694	0.305	1.415	0.335	0.049	0.392	0.068	0.487	4.215	0.118	0.371	0.058	0.403	0.055	10.420	0.021	0.045
	2-1	PS4	2nd	6,215.84	0.262	1.371	0.325	1.577	0.469	0.179	0.477	0.096	0.745	6.645	0.165	0.520	0.086	0.497	0.067	13.483	0.017	0.166
	2-1	PS4	2nd	6,215.84	0.296	1.114	0.207	0.926	0.234	0.105	0.248	0.045	0.337	3.021	0.081	0.243	0.036	0.229	0.038	7.161	0.014	0.097
	2-1	PS4	2nd	6,215.84	0.208	0.789	0.153	0.691	0.189	0.073	0.173	0.035	0.242	2.305	0.055	0.213	0.030	0.221	0.032	5.409	0.010	0.068
	2-3	ZS102	2nd	6,146.69	0.318	1.011	0.190	0.837	0.196	0.076	0.193	0.034	0.263	2.781	0.061	0.171	0.022	0.132	0.019	6.304	0.013	0.070
	4-6	PS7	4th	7,245.68	0.649	1.113	0.178	0.674	0.148	0.052	0.182	0.024	0.155	1.896	0.030	0.070	0.008	0.036	0.005	5.219	0.014	0.048
SD	2-7	PT105	2nd	5,940.00	1.298	3.081	0.559	2.577	0.639	0.189	0.657	0.103	0.648	3.838	0.131	0.330	0.044	0.228	0.037	14.358	0.039	0.175
	2-7	PT105	2nd	5,940.00	2.770	6.806	1.279	5.293	1.072	0.478	1.157	0.149	0.822	6.711	0.140	0.331	0.032	0.145	0.018	27.203	0.086	0.443

Num, sample number; Form, formation; MD, thrombolitic matrix dolomite; IFC, isopachous fibrous cement; FSC, fine crystalline spar cement; M-CD, medium to coarse crystalline dolomite cement; SD, saddle dolomite cement; Second, Second Member of Dengying Formation; Fourth, Fourth Member of Dengying Formation; ND, not detected.

TABLE 3 Carbon and oxygen stable isotopes for thrombolitic matrix and different types of cements from the Precambrian Dengying Formation in the central Sichuan Basin.

Type	Num	WellID	Form	Depth	$\delta^{13}C_{VPDB}$	$\delta^{18}O_{VPDB}$	Type	Num	WellID	Form	Depth	$\delta^{13}C_{VPDB}$	$\delta^{18}O_{VPDB}$
				m	‰	‰					m	‰	‰
MD	2-1	PS4	2nd	6,215.84	2.93	−1.45	FSC	4-1	DB1	4th	6,405.61	2.38	−8.72
	2-3	ZS102	2nd	6,146.69	1.11	−2.45		4-6	PS7	4th	7,245.68	2.63	−7.57
	2-3	ZS102	2nd	6,146.69	1.74	−3.17		4-8	PS8	4th	7,050.89	0.76	−6.09
	2-7	PT105	2nd	5,940.00	2.68	−3.33		4-8	PS8	4th	7,050.89	2.40	−7.50
	2-7	PT105	2nd	5,940.00	1.60	−3.30	M-CD	2-1	PS4	2nd	6,215.84	3.16	−7.06
	2-9	ZS102	2nd	6,044.48	1.80	−4.10		2-1	PS4	2nd	6,215.84	1.70	−6.86
	4-1	DB1	4th	6,405.61	2.27	−3.93		2-1	PS4	2nd	6,215.84	2.33	−7.61
	4-4	DB1	4th	6,407.16	2.50	−4.74		2-3	ZS102	2nd	6,146.69	2.69	−6.71
	4-6	PS7	4th	7,245.68	3.38	−3.75		2-7	PT105	2nd	5,940.00	2.70	−6.90
	4-7	PS2	4th	7,780.61	1.04	−3.21		2-8	ZS102	2nd	6,055.92	2.17	−8.78
	4-8	PS8	4th	7,050.89	1.95	−2.89		2-9	ZS102	2nd	6,044.48	2.50	−7.00
	4-8	PS8	4th	7,050.89	1.20	−4.50		4-1	DB1	4th	6,405.61	1.40	−6.98
IFC	2-1	PS4	2nd	6,215.84	2.79	−4.20		4-1	DB1	4th	6,405.61	1.15	−5.86
	2-3	ZS102	2nd	6,146.69	1.29	−4.34		4-6	PS7	4th	7,245.68	1.13	−7.88
	2-3	ZS102	2nd	6,146.69	2.39	−2.85		4–7	PS2	4th	7,780.61	0.90	−9.65
	2-7	PT105	2nd	5,940.00	3.73	−5.47		4–8	PS8	4th	7,050.89	1.78	−8.54
	2-7	PT105	2nd	5,940.00	2.10	−3.70	SD	2-1	PS4	2nd	6,215.84	1.66	−10.89
	2-8	ZS102	2nd	6,055.92	1.09	−4.16		2-3	ZS102	2nd	6,146.69	0.43	−11.87
	2-9	ZS102	2nd	6,044.48	0.70	−5.30		2-7	PT105	2nd	5,940.00	2.12	−9.63
	4-1	DB1	4th	6,405.61	1.77	−5.62		2-7	PT105	2nd	5,940.00	0.70	−10.80
	4-1	DB1	4th	6,405.61	2.26	−6.43		2-8	ZS102	2nd	6,055.92	1.06	−10.89

(Continued on the following page)

10.3389/feart.2024.1407400

TABLE 3 (*Continued*) Carbon and oxygen stable isotopes for thrombolitic matrix and different types of cements from the Precambrian Dengying Formation in the central Sichuan Basin.

Type	Num	WellID	Form	Depth	$\delta^{13}C_{VPDB}$	$\delta^{18}O_{VPDB}$	Type	Num	WellID	Form	Depth	$\delta^{13}C_{VPDB}$	$\delta^{18}O_{VPDB}$
				m	‰	‰					m	‰	‰
IFC	4-4	DB1	4th	6,407.16	1.30	−6.91	SD	2-9	ZS102	2nd	6,044.48	0.00	−9.91
	4-7	PS2	4th	7,780.61	1.95	−5.72		2-9	ZS102	2nd	6,044.48	1.80	−13.20
	4-8	PS8	4th	7,050.89	1.31	−4.14		4-1	DB1	4th	6,405.61	1.26	−10.15
	4-8	PS8	4th	7,050.89	1.65	−4.71		4-4	DB1	4th	6,407.16	1.40	−12.13
FSC	2-3	PT105	2nd	6,146.69	2.52	−8.87		4-6	PS7	4th	7,245.68	1.54	−8.72
	2-7	ZS102	2nd	5,940.00	0.77	−6.68		4-8	PS8	4th	7,050.89	0.77	−9.06
	2-8	ZS102	2nd	6,055.92	2.87	−6.62		4-8	PS8	4th	7,050.89	1.21	−12.00

MD, thrombolitic matrix dolomite; IFC, isopachous fibrous cement; FSC, fine crystalline spar cement; M-CD, medium to coarse crystalline dolomite cement; SD, saddle dolomite cement; Second, Second Member of Dengying Formation; Fourth, Fourth Member of Dengying Formation.

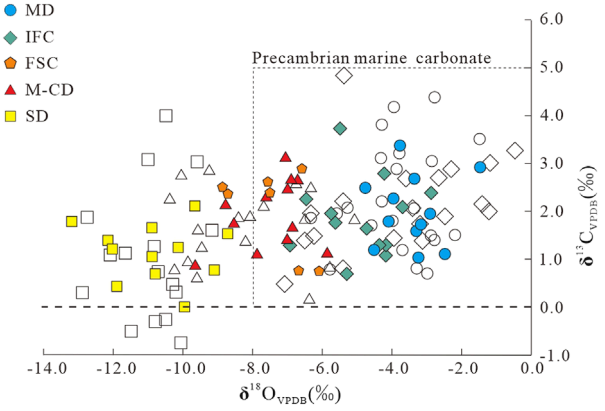

FIGURE 8
Carbon and oxygen stable isotope data on the thrombolitic matrix and different types of cements observed in the thin sections from the Precambrian Dengying Formation. Estimated isotopic values of Neoproterozoic marine carbonate are from Halverson et al. (2010) and Tahata et al. (2013). Data points not filled with color are from Ding et al. (2019) and Xu et al. (2022). MD, thrombolitic matrix dolomite; IFC, isopachous fibrous cement; FSC, fine crystalline spar cement; M-CD, medium-to-coarse crystalline dolomite cement; SD, saddle dolomite cement.

relationship between thrombolites and stromatolites (Figures 3A, B) corresponds well to the pattern described for the Messinian microbialites in the western Mediterranean (Suarez-Gonzalez et al., 2019b). The mesostructural succession of thrombolites from laminated to massive (Figures 3C–F) indicates a shallowing-upward sedimentary environment (Suarez-Gonzalez et al., 2019b). The microclots in the DCT, which occur at the beginning of the sedimentary succession, are spherical microbial communities (Harwood and Sumner, 2012) with commonly well-developed growth-framework pores between these clot particles (Figures 4A, E, 5A). The boundaries of DRCT and DICT microclots show a diffuse transition, and dark gray folded microclots are also observed within some microclots (Figures 4B–D). This suggests that the organic matter of the microclots began to degrade during deposition and was then preserved through lithification. Microclot morphology and structure are influenced by variations in microbial community composition and environmental conditions, as well as physical changes during sedimentation and diagenesis, which can induce microclot deformation and transformation, as observed in Neoproterozoic Beck Spring dolomite and modern microbialites in Shark Bay, Australia, and the Bahamas (Riding, 2000; Reid et al., 2024). The spherical and sub-spherical microclot structures and laminated structures of the CCT suggest diversity of microbial ecology and may have resulted from the simultaneous occurrence of multiple types of microbial communities that flourished through natural selection in paleoecology (Pratt and James, 1982; Harwood and Sumner, 2012). The inherent stability of microclot fabrics and the high connected growth-framework porosity facilitate fluid migration and promote the later flow of diagenetic fluids and the formation of selective dissolution to form secondary dissolution pores (Harwood Theisen and Sumner, 2016). Therefore, thrombolites provide optimal conditions for reservoir formation

and are dominant in the distribution of high-quality reservoirs within microbialite facies.

5.2 Reservoir modification by multiple diagenetic fluids

The Precambrian thrombolitic dolomites of the central Sichuan Basin include two intervals of high-quality reservoirs. These reservoirs consist of microbial mounds and shoal facies, capped by unconformity surfaces, which correspond with the Dengying Second and Fourth Members. Based on the petrographic characteristics of the previously described diagenetic products and their elemental and stable isotopic composition, the timing of diagenetic events of the Precambrian Dengying Formation can be inferred in the context of syngenetic-eogenetic, epigenetic, shallow burial, and middle to deep burial diagenetic environments. Moreover, the mineral paragenetic sequence and diagenetic evolution patterns were established (Figure 11; Figure 12).

5.2.1 Syngenetic–eogenetic environment

At the syngenetic-eogenetic stage, the dolomicrite crystals found in the thrombolitic microclots may indicate either early dolomitization (Figures 4A–H, 5A–D), likely facilitated by microbial activities or may indicate direct precipitation of dolomite of microbial origin, as evidenced by dolomitized EPs and spherulites (Figures 5G, H) (Yuan et al., 2022; Mather et al., 2023). Early bacterial sulfate reduction below the water-sediment interface can promote the early diagenetic formation of dolomite (Burns et al., 2000; Baldermann et al., 2025). Most likely, the cryptocrystalline micritic precursors of the dolomites (e.g., calcite, aragonite, high-Mg calcite, or nonstoichiometric and disordered protodolomite) precipitated from seawater or marine porewaters (Chang et al., 2020; Wang J. et al., 2020). Furthermore, several studies have reported the occurrence of dolomitized EPs, even bacteria-like fossils, dolomitic nanometer-filament aggregates, and possible organic residue from archaebacteria, all of which were observed under ultramicroscopes in the Dengying Formation at other locations (Zhou et al., 2020; Wang et al., 2022; Xu et al., 2022; Azizi et al., 2023). These findings provide compelling evidence that microorganisms have played an important role in either the syngenetic primary dolomite precipitation in the thrombolites or the very early microbial dolomitization during eogenesis (Hood et al., 2011). Grotzinger and Al-Rawahi (2014) proposed that up to 50% of the initial porosity of the thrombolites was preserved by early dolomitization before significant compaction in the Ara Group, Sultanate of Oman. Consequently, either of the two dolomite formation processes, the direct microbial-mediated dolomite precipitation or the early microbial dolomitization, preserved the thrombolite fabrics and growth-framework pores (Figures 4A, B) (Zhang et al., 2014; Shen et al., 2019).

On the other hand, the isopachous fibrous cements with needle-like crystals (Figure 12A) suggest that these cements were mineralogically primary aragonite or high-Mg calcite (Cui et al., 2019) that was later mimically dolomitized. This cement typically fills less than 10% of the open porosity. The isopachous fibrous cement typically occurs in the marine phreatic environment and has been widely used to constrain paleoseawater chemistry (Longman, 1980; Hood et al., 2011; Zhao et al., 2021). Isopachous fibrous cement with alternating light and dark layers formed botryoidal structures with a thickness of millimeters to centimeters (Figure 6D) (Lu et al., 2023). The presence of high Na+K, Ba, and negative Ce anomalies, along with relatively low Fe and Mn in the thrombolitic dolomicrite matrix and isopachous fibrous cement (Table 4; Figures 8, 9, 10A) suggests precipitation from oxidizing, saline fluids (Byrne and Sholkovitz, 1996; Bau and Dulski, 1999). The negative $\delta^{18}O$ values of both thrombolites and isopachous fibrous cement rule out hypersaline or high saline fluids, whose precipitates would show positive $\delta^{18}O$ values (Figure 8) (Land, 1985). The mean Sr contents of both are low compared to modern marine precipitates (Carpenter and Lohmann, 1992) and modern dolomites of proposed bacterial-mediated marine and evaporative-marine origin, which may exceed 600 ppm (Banner, 1995), suggesting significant loss of Sr during diagenesis. The low total rare earth element concentrations (ΣREE) of the isopachous fibrous cement suggest that the fibrous cement may have undergone early dolomitization either in a marine environment shortly after precipitation or in the very shallow burial zone driven by modified pore seawater. Both possibilities are consistent with the normal-marine positive $\delta^{13}C$ and negative $\delta^{18}O$ values. These stable isotope values are characteristic of Precambrian marine carbonates (Figures 8, 10A) (Halverson et al., 2010; Tahata et al., 2013). The mean $\delta^{18}O$ values of the fibrous cement are slightly more negative than those precipitated from normal marine waters, reinforcing the shallow burial diagenetic environment for the mimic dolomitization of these fibrous cements. However, the dolomitization process for this cement is not well-understood, given that the positive $\delta^{13}C$ values it presents rule out bacterial activity, and the quite-negative $\delta^{18}O$ values rule out seepage reflux involving hypersaline fluids. On the other hand, it is known that the Precambrian was a time dominated by "aragonite and dolomite seas" and, therefore, the seawater conditions differed substantially from those of today, with high Mg/Ca ratios and alkalinity (Li et al., 2023a). In these Precambrian aragonite and dolomite seas, fibrous aragonite or high-Mg calcite cements have formed penecontemporaneously with sedimentation (Hood et al., 2011; Cui et al., 2019; Zhou et al., 2020). However, the relatively high Mg/Ca ratios and alkalinity of the seawater may have also promoted the early dolomitization of the marine precipitates shortly after precipitation in the seafloor or/and during shallow burial from marine pore fluids, or alternatively, according to some authors, may even have precipitated directly as dolomite (Table 1; Figure 9F) (Li et al., 2023a). Therefore, both the thrombolitic dolomite and the fibrous dolomitized cement reflect either very early dolomitization that possibly occurred from the coeval seawater or seawater-type fluids during eogenesis (Wang J. et al., 2020) or they reflect primary dolomite precipitation in the sea floor. In this study, we have opted for the first proposal, which is the early mimic substitution of the primary aragonite or calcite by dolomite. The isopachous fibrous cements formed via rapid syntaxial replacement by dolomite better preserved the fibrous aragonite or high-Mg calcite habit (Sibley, 1991). Dolomitized aragonite and high-Mg calcite cements can retain their botryoidal form (Hood et al., 2011). The well-preserved fibrous habit of the precursor mineralogy suggests that the mimic dolomitization occurred during early shallow burial (Sibley, 1991; Zhao et al., 2021).

TABLE 4 Mineral paragenesis of diagenetic products and their characteristics for the thrombolitic dolomite reservoirs of the Precambrian Dengying Formation in the central Sichuan Basin.

Mineral	Crystal morphology	CL	Geochemistry		Stable isotopes		Figure
			Trace element	REE	$\delta^{13}C_{VPDB}$, ‰	$\delta^{18}O_{VPDB}$, ‰	
MD	Micrite crystal	Weak red	High Na, K, and Ba; low Fe, Mn, and Sr	Negative Ce; flat REE Pattern	(1.04, 3.38)	(−4.74, −1.45)	Figure 5A
IFC	Fibrous	Dull to blotchy	High Na and K; low Fe, Mn, and Sr	Negative Ce; low ΣREE	(0.70, 3.73)	(−6.91, −2.85)	Figures 5A, 6D
FSC	Fine particle	Red/weak red	Low Na, K, and Sr; low Fe and Mn; low Fe/Mn ratio	HREE-rich	(0.76, 2.87)	(−8.87, −6.09)	Figures 5C, D, F
M-CD	Euhedral	Weak red	Low Na and K; Low Fe and Mn	Positive Eu; HREE-rich	(0.90, 3.16)	(−9.65, −5.86)	Figure 5A
SD	Non-planar subhedral and sweeping extinction	Bright red	High Fe and Mn; low Na, K, and Sr	Positive Eu; MREE-rich	(0.00, 2.12)	(−13.2, −8.72)	Figures 5C, D, F

MD: thrombolitic matrix dolomite; IFC: isopachous fibrous cement; FSC: fine crystalline spar cement; M-CD: medium to coarse crystalline dolomite cement; SD: saddle dolomite cement.

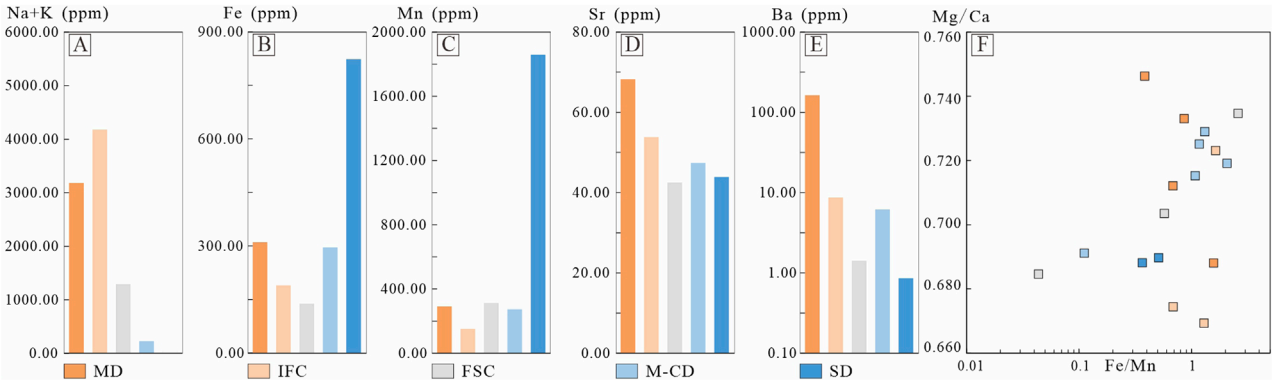

FIGURE 9
Values of the main trace elements analyses by LA-ICP-MS of thrombolitic matrix and cements observed from thin sections of the Precambrian Dengying Formation. **(A–E)** Parts per million concentrations of Na+K, Fe, Mn, Sr, and Ba in different dolomite types and **(F)** scatter plots of Fe/Mn ratios and Mg/Ca ratios. MD, thrombolitic matrix dolomite; IFC, isopachous fibrous cement; FSC, fine crystalline spar cement; M-CD, medium-to-coarse crystalline dolomite cement; SD, saddle dolomite cement.

5.2.2 Epigenetic environment

At the epigenetic stage, the topographic uplift caused by the episodic Tongwan tectonic event formed unconformities, and the structural reactivation in the late Precambrian resulted in subaerial exposure and erosion at the tops of the Dengying Second and Fourth Members, leading to erosion and karstification in a meteoric environment (Figures 2B, 11). These episodic exposures resulted in meteoric leaching and dissolution along the growth-framework pores, affecting the matrix and fibrous cements. As a result of extensive non-fabric selective dissolution, new pores, vugs, and karst breccias were formed (Figures 5C, 6B, 12B). The karstification mainly occurred within a depth range of 100 m beneath the exposure surface, while the rest of the strata were either minimally affected or unaffected (Jin et al., 2020). Similar characteristics have also been observed in microbialitic reservoirs from other regions, such as the uppermost Precambrian Qigebrak Formation in the Tarim Basin, China, the Permian upper Dalan Formation and the Triassic Kangan Formation in the Zagros Basin, and the upper Jurassic Smackover Formation in southwest Alabama (Mancini et al., 2006; Jafarian et al., 2018; Chen et al., 2023). The wide distribution of the millimeter to centimeter dissolution vugs and karst breccia in the cores at the top of the Dengying Second and Fourth Members indicates substantial weathering and karstification (Figures 1B, 3D, F, 5C) (Jin et al., 2020). This is consistent with the petrological and geochemical evidence of meteoric seepage and pendant cements related to the percolation of meteoric water, as found by Xu et al. (2022) and Yang et al. (2023) in the microbial reservoir of the Dengying Formation in the study area.

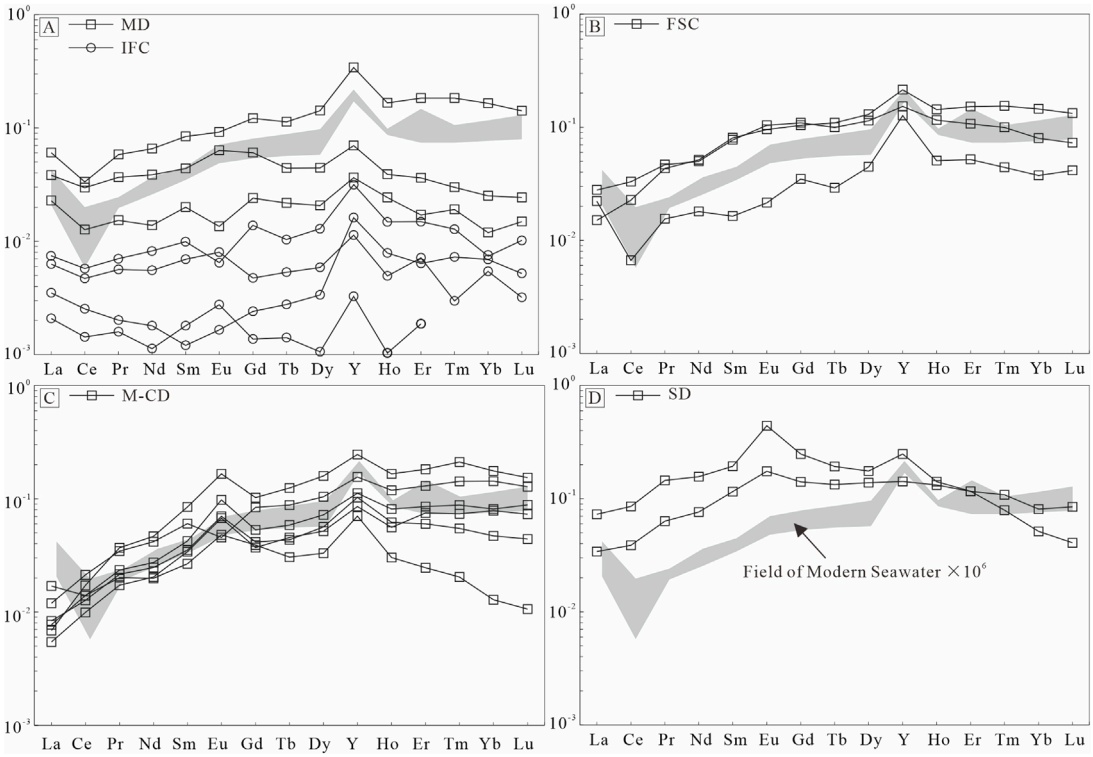

FIGURE 10
PAAS-normalized REE+Y distribution patterns of **(A)** thrombolitic matrix dolomite (MD), isopachous fibrous cement (IFC), **(B)** fine crystalline spar cement (FSC), **(C)** medium-to-coarse crystalline dolomite cement (M-CD), and **(D)** saddle dolomite cement (SD) from the Precambrian Dengying Formation in the central Sichuan Basin. PAAS from McLennan (1989).

5.2.3 Shallow burial environment

In the shallow burial environment, the thrombolitic dolomite reservoir experienced significant porosity and permeability reduction, ranging from 10% to 30%, due to physical compaction and fine crystalline spar cementation (Figures 11, 12C). Fine crystalline spar cement filled the growth-framework pores after the isopachous fibrous cement or directly filled the dissolution pores, vugs, and the spaces between the karst breccias (Figures 5A, B). This type of cement initially formed as fine crystalline low-Mg calcite and then subsequently underwent dolomitization during shallow burial, probably from mixed marine and residual meteoric waters (Lukoczki et al., 2020; Murray et al., 2021). Geochemically, these cements exhibit low Na+K, Fe, and Mn contents with the lowest Fe/Mn ratio, negative Ce anomalies, and heavy rare earth element (HREE) enrichment (Table 4; Figures 9, 10B), indicating that the cement precipitated from residual meteoric water in the shallow burial environment (Yang et al., 2023). During the later shallow burial, the fine crystalline spar cement underwent dolomitization subsequent to the cementation (Nelson and Read, 1990). Diagenetic fluids transited from marine to formation water, a relatively closed system that underwent alterations due to variations in geothermal gradients and compaction (Peng et al., 2018; Lukoczki et al., 2020). Consequently, the Mg^{2+} ion in the fluid reacted with precursor minerals and low-Mg calcite to form new dolomite in the shallow burial environment.

5.2.4 Middle and deep burial environment

With progressive burial, medium to coarse crystalline dolomite cement precipitated, exhibiting low Na+K, Ba, HREE enrichment, and positive Eu anomalies. They are dark red under CL. These are geochemical fingerprints that indicate precipitation from fluids that are inconsistent with a marine environment (Table 4; Figures 9, 10C). Compared to the matrix and isopachous fibrous cement, medium to coarse crystalline dolomite cement exhibits negatively shifted $\delta^{18}O$ values (Figure 8), indicating oxygen isotope fractionation associated with increasing temperature during deeper burial (Anderson and Arthur, 1983). Saddle dolomite cement occurs within pores, vugs, fractures, or spaces between breccias, occupying more than 30% of the remaining pore space (Figures 5C, D). Compared to other cements, saddle dolomite cement has the lowest Na+K and Ba, extremely high Fe and Mn, high Fe/Mn ratios, is bright red under CL, and has strongly negative $\delta^{18}O$ values (Table 4; Figures 5C, 8, 9, 10D). These are characteristic of precipitation from hot basinal brines migrating along fractures and precipitating rapidly (Feng et al., 2017). The high temperatures facilitated the reductive incorporation of Eu^{2+} into the dolomite lattice (Bolhar and Van Kranendonk, 2007). The enrichment of middle rare earth elements (MREEs) suggests the precipitation of saddle dolomite cement from pore fluids where the preferential adsorption of light rare earth elements (LREE) and HREE onto dissolving Fe-Mn oxides or hydroxides released MREE (Figure 10) (Bayon et al., 2011). Furthermore, chemical compaction and recrystallization

10.3389/feart.2024.1407400

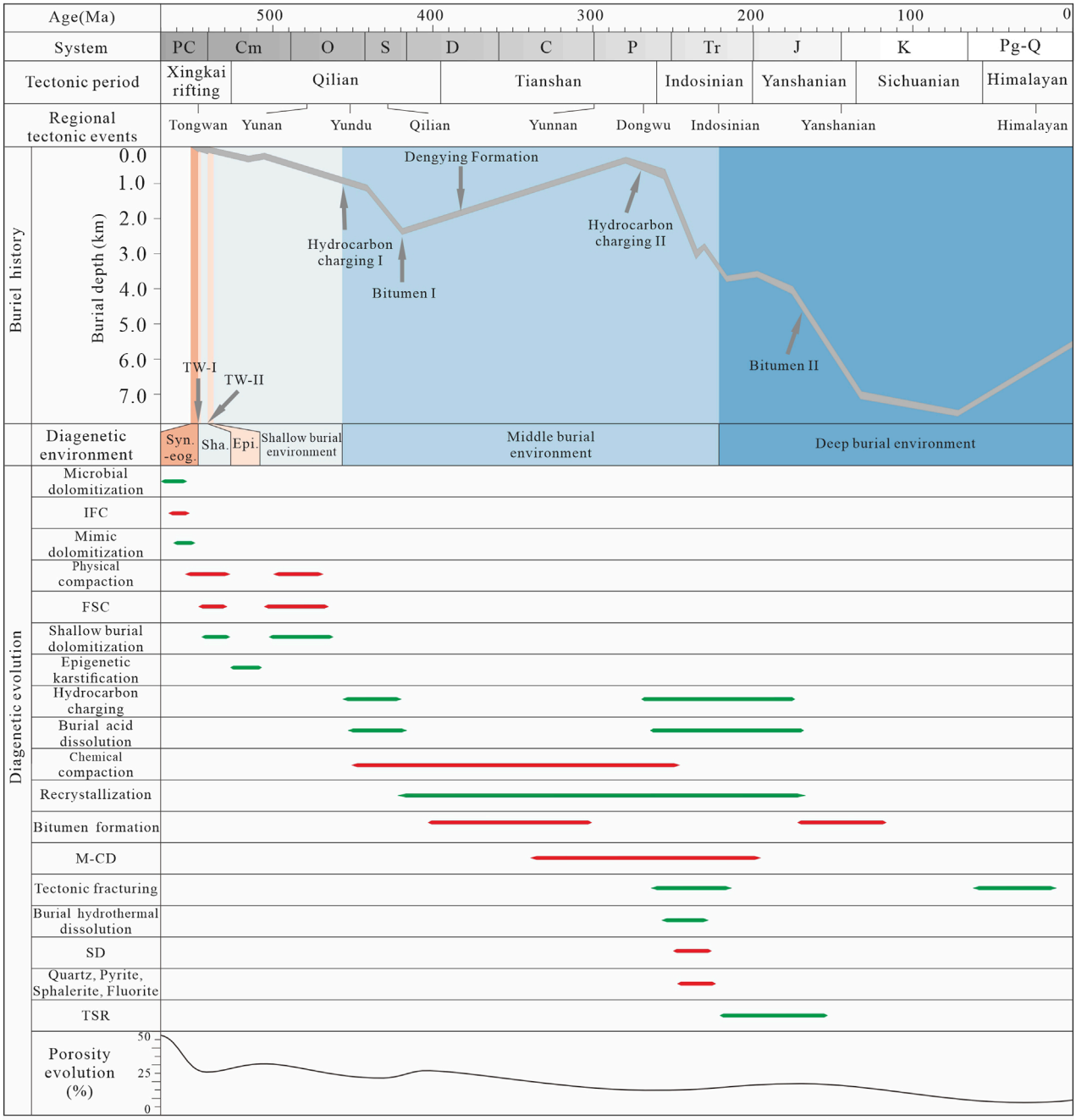

Syn.-eog.= Syngenetic-eogenetic environment, Sha.= Shallow burial environment, Epi.= Epigenetic environment, IFC= Isopachous fibrous cement, FSC= Fine crystalline spar cement, M-CD= Medium to coarse crystalline dolomite cement, SD= Saddle dolomite cement, TSR= Thermochemical sulfate reduction.

FIGURE 11
Burial evolution history and diagenetic sequence of the thrombolitic dolomite reservoirs of the Precambrian Dengying Formation in the central Sichuan Basin. The green bars in the diagenetic sequence are diagenetic events of pore creation that favor reservoir development, while the red bars represent diagenetic events and products that destroy or close porosity. PC, Precambrian; Cm, Cambrian; O, Ordovician; S, Silurian; D, Devonian; C, Carboniferous; P, Permian; Tr, Triassic; J, Jurassic; K, Cretaceous; Pg, Paleogene; Q, Quaternary; TW-I, episode I of the Tongwan uplift tectonic event; TW-II, episode II of the Tongwan uplift tectonic event. Different diagenetic environments are projected onto the burial evolution history through color blocks.

during middle and deep burial had a relatively weak impact on the reservoir quality of the thrombolitic dolomicrite within the thrombolitic microclots (Wang et al., 2000).

Additionally, hydrocarbon charging with fluids containing organic acids and later thermochemical sulfate reduction (TSR) has been confirmed to dissolve thrombolites and create secondary pores in burial mesogenetic environments and re-precipitation in adjacent geological bodies (Chen et al., 2017; Rosales et al., 2018). This is consistent with the irregular dissolution of medium to coarse crystalline dolomite cement, the intraparticle pores within

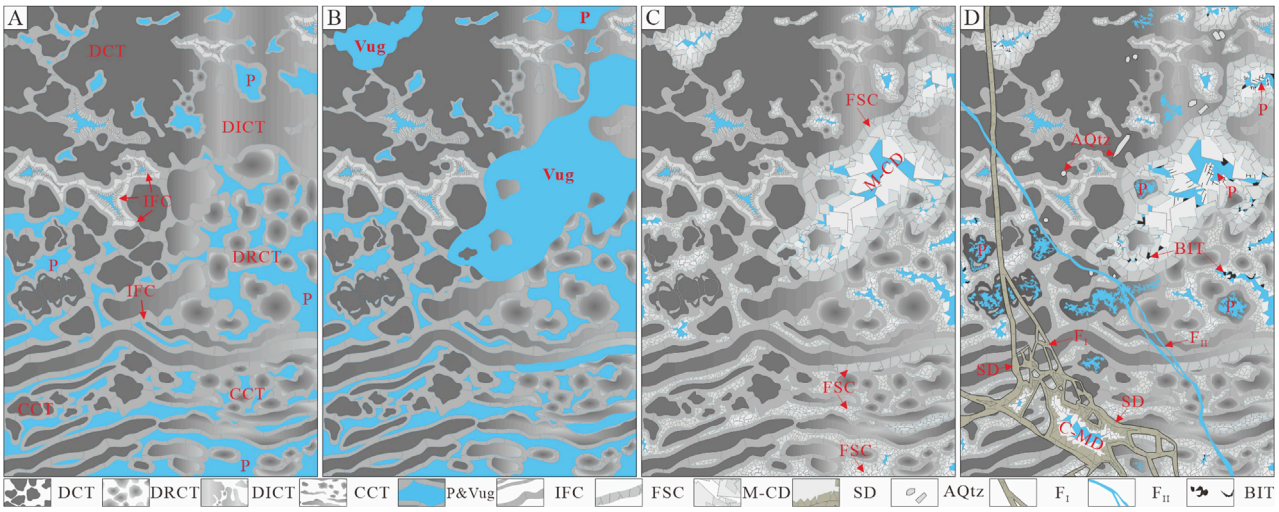

FIGURE 12
Evolution sketch of thrombolitic dolomite reservoir porosity for the Precambrian Dengying Formation in the central Sichuan Basin. **(A)** Syngenetic–eogenetic stage with four types of thrombolites and their growth-framework pores (P) cemented with IFC; **(B)** epigenetic stage with meteoric dissolution pores and vugs; **(C)** burial stage with pores and vugs cemented by FSC, M-CD; **(D)** tectonic fracturing and hydrocarbon charging stage with SD, bitumen (BIT) filling in the pores and fractures, and some authigenic quartz (AQtz) being within the microclots. Intraparticle dissolution pores occurred within some microclots, and rarely, M-CD was dissolved by organic acids (P). Hydrothermal events and minerals like quartz (Qtz), pyrite (Py), sphalerite (SP), and fluorite (FL), filling fractures, pores, and vugs are not depicted. MD, thrombolitic matrix dolomite; IFC, isopachous fibrous cement; FSC, fine crystalline spar cement; M-CD, medium-to-coarse crystalline dolomite cement; SD, saddle dolomite cement; F_I, earlier filled fracture; F_{II}, later fracture unfilled or partially filled with quartz; BIT, bitumen.

the microclots half-filled with bitumen (Figures 6B, C), and the high H_2S content of the produced natural gas (Wen et al., 2023). The bitumen plugged the reservoir porosity and decreased the porosity and permeability of the thrombolitic dolomite reservoir (Figures 5D, F) (Li et al., 2023b). In addition, bitumen residues observed within the precipitation zones of the medium to coarse crystalline dolomite cement with irregular crystal surfaces (Figures 6B, D) indicate that bitumen may have inhibited later cementation and facilitated the preservation of porosity. Authigenic quartz particles with dirty crystal surfaces and non-directional distributions, commonly developed within DCT (Figures 4A, E, 5J), also occurred in the deep burial environment.

5.3 Reservoir modification by tectonic fracturing

Apart from the tectonic uplift and erosion caused by the episodic Tongwan tectonic events, the development of the thrombolitic reservoir has also been significantly influenced by the tectonic fractures formed through two later stages of tectonic events, the Dongwu and Himalayan tectonic events (Figure 11). The fractures improve the permeability of low-porosity thrombolitic reservoirs (Figure 7B). Previous studies on the porosity-permeability of the Dengying Formation reservoirs in the central Sichuan Basin have shown that fractures play an important role in determining reservoir porosity and permeability, forming fracture-porosity-type reservoirs (Wang L. et al., 2020).

The occurrence of later fracturing and tectonic breccias with infillings of hydrothermal minerals such as saddle dolomite, quartz, pyrite, sphalerite, and fluorite within the Dengying Formation thrombolites serves as clear evidence that tectonic features modified the reservoir (Figures 3E, 4A–C, G, 5C–F, 6E). This metal-rich hydrothermal fluid charging may be related to the Emeishan basalt eruption triggered by the Dongwu tectonic event during the Late Permian to Early Triassic (Huang et al., 2022; Deng et al., 2022), which resulted in a large number of fractures (F_I) (Figures 3E, 4A–C, 11). Tectonic fractures formed during this tectonic event provide pathways for the flow of hydrothermal fluids, especially along tectonic shear fractures (Wen et al., 2022). Under such conditions, the reservoirs underwent tectonic and hydrothermal modifications, resulting in the formation of fractures and secondary non-fabric selective dissolution pores to form a porous hydrothermal dolomite reservoir. Additionally, chemicals and metals carried by the hydrothermal fluids may precipitate as new minerals within the reservoirs. This type of reservoir in the central Sichuan Basin is commonly distributed in a linear or belt-like manner along strike-slip faults (Feng et al., 2017). Tectonic fractures formed by the Dongwu tectonic event have been mostly filled with various types of cement or bitumen, resulting in ineffective or low porosity (Zhou et al., 2020). In contrast, the later fractures (F_{II}) formed during the Himalayan period are unfilled or only partially filled (Figures 3E, 4B–C, G, 6E), improving the connectivity of reservoir spaces.

As a result of all this, after undergoing various stages of tectonic fracturing and diagenetic modification, such as epigenetic karst, multistage fluid cementations, and hydrothermal dissolution, the Precambrian Dengying Formation in the study area has developed thrombolitic reservoirs with low porosity and ultra-low permeability. However, the superposition of stacked microbial

mounds and shoals in the platform on the rifted margin (Xia et al., 2024), with effective connections between growth-framework pores, dissolution vugs, and network fractures, provides the necessary conditions for the formation of high-quality fracture-porosity or vug-porosity type dolomite reservoirs and demonstrates great potential for large-scale oil and gas exploration.

6 Conclusion

This study helps to understand the reservoir characteristics and development of thrombolitic dolomites from the Precambrian Dengying Formation in the central Sichuan Basin, southwestern China. Four types of thrombolites were identified based on microclot texture. The reservoir porosity is dominated by primary growth-framework pores and secondary dissolution pores and vugs, followed by intraparticle dissolution pores and open tectonic fractures. All these types of primary and secondary pores were extensively filled by several generations of carbonate cements and hydrothermal minerals, resulting in overall low porosity and ultra-low permeability. Within the differentiated thrombolite facies, diffuse microclots are particularly favorable for reservoir development. Secondary porosity is mainly derived from meteoric dissolution during tectonic uplifting events that exposed the reservoir subaerially. These emersion events resulted in intense karstification and erosion of the reservoirs before being buried again up to a maximum depth of approximately 7 km during deep burial. The dissolution by fluids rich in organic acids, TSR, and deep hydrothermal fluids occurred during the deep burial and has made certain contributions to the development of reservoirs, but it is mainly reflected in the preservation and adjustment of pores. Tectonic fracturing has effectively enhanced reservoir connectivity, while intense cement and mineral precipitation and bitumen infilling decreased the porosity. The reservoir quality has been significantly diminished by multistage cementation and physical and chemical compaction. The reservoirs of the Precambrian Dengying Formation in the central Sichuan Basin are mainly developed in the middle to top intervals of the Dengying Second and Fourth Members, where the thrombolitic dolomite with high growth-framework porosity underwent meteoric dissolution in relation to subaerial dissolution related with the tectonic uplift during postdepositional Tongwan tectonic events.

Based on the diagenetic sequence and elemental and stable isotope geochemistry of the different cement types, this study has reconstructed the diagenetic and burial history and established a reservoir evolution model for thrombolitic dolomites in the Precambrian Dengying Formation. These findings provide a crucial workflow and practical insights for understanding the mechanisms of development of thrombolitic reservoirs and can help to predict high-quality microbialitic dolomite reservoirs in deep and ultra-deep hydrocarbon exploration. The occurrence of thrombolites, often mixed with stromatolites and other microbialites, presents challenges at the meso-micro scale in terms of studying their sedimentary environments, microbial community evolution, reservoir petrology, and diagenesis. Further research should integrate modern and fossil microbialites to analyze in detail the controls on thrombolitic reservoir development and to clarify the interactions between microbial communities, paleoecology, and reservoir development.

Data availability statement

The original contributions presented in the study are included in the article/supplementary material; further inquiries can be directed to the corresponding author.

Author contributions

YL: conceptualization, funding acquisition, project administration, resources, and writing–review and editing. BZ: funding acquisition, resources, and writing–review and editing. GZ: investigation and writing–original draft. RT: project administration and writing–original draft. HL: investigation and writing–original draft. CL: project administration and writing–original draft. XC: investigation and writing–original draft. DC: investigation and writing–original draft. XL: conceptualization, funding acquisition, validation, visualization, writing–review and editing, and writing–original draft. CZ: visualization and writing–original draft. MF: writing–review and editing.

Funding

The author(s) declare that financial support was received for the research, authorship, and/or publication of this article. This study was financially supported by the Major Science and Technology Projects of PetroChina (Grant No. 2021DJ0204) and the PetroChina Southwest Oil and Gasfield Company (Grant No. XNS-KYY CL2022-029).

Acknowledgments

The authors thank a reviewer and Pablo Suarez-Gonzalez for critical and constructive reviews that improved the original manuscript. They also acknowledge Idoia Rosales, Associate Editor, for handling the manuscript and providing editorial guidance.

Conflict of interest

Authors YL, BZ, GZ, HL, CL, XC, and DC were employed by the PetroChina Southwest Oil and Gasfield Company.

Author RT was employed by the Exploration Division of PetroChina Southwest Oil and Gasfield Company.

The remaining authors declare that the research was conducted in the absence of any commercial or financial relationships that could be construed as a potential conflict of interest.

Publisher's note

References

Aitken, J. D. (1967). Classification and environmental significance of cryptalgal limestones and dolomites, with illustrations from the Cambrian and Ordovician of southwestern Alberta. *J. Sediment. Res.* 37, 1163–1178. doi:10.1306/74D7185C-2B21-11D7-8648000102C1865D

Altermann, W., and Corcoran, P. L. (2002). *Precambrian sedimentary environments: a modern approach to ancient depositional systems* (Oxford: Blackwell Science).

Anderson, T. F., and Arthur, M. A. (1983). "Stable isotopes of oxygen and carbon and their application to sedimentologic and paleoenvironmental problems," in *Stable isotopes in sedimentary geology*. Editors M. A. Arthur, T. F. Anderson, I. R. Kaplan, J. Veizer, and L. S. Land (Claremore, Oklahoma, United States: SEPM Society for Sedimentary Geology). doi:10.2110/scn.83.01.0000

Arp, G., Hofmann, J., and Reitner, J. (1998). Microbial fabric formation in spring mounds ("microbialites") of alkaline salt lakes in the Badain Jaran sand sea, PR China. *Palaios* 13, 581–592. doi:10.2307/3515349

Azizi, A., Albani, A. E., Bakhouche, A. E., Vinn, O., Bankole, O. M., Fontaine, C., et al. (2023). Early biomineralization and exceptional preservation of the first thrombolite reefs with archaeocyaths in the lower Cambrian of the western Anti-Atlas, Morocco. *Geol. Mag.* 160, 428–443. doi:10.1017/S0016756822001017

Baldermann, A., Deditius, A. P., Dietzel, M., Fichtner, V., Fischer, C., Hippler, D., et al. (2015). The role of bacterial sulfate reduction during dolomite precipitation: implications from Upper Jurassic platform carbonates. *Chem. Geol.* 412, 1–14. doi:10.1016/j.chemgeo.2015.07.020

Banner, J. L. (1995). Application of the trace element and isotope geochemistry of strontium to studies of carbonate diagenesis. *Sedimentology* 42, 805–824. doi:10.1111/j.1365-3091.1995.tb00410.x

Bau, M., and Dulski, P. (1999). Comparing yttrium and rare earths in hydrothermal fluids from the Mid-Atlantic Ridge: implications for Y and REE behaviour during near-vent mixing and for the Y/Ho ratio of Proterozoic seawater. *Chem. Geol.* 155, 77–90. doi:10.1016/S0009-2541(98)00142-9

Bayon, G., Birot, D., Ruffine, L., Caprais, J.-C., Ponzevera, E., Bollinger, C., et al. (2011). Evidence for intense REE scavenging at cold seeps from the Niger Delta margin. *Earth Planet. Sci. Lett.* 312, 443–452. doi:10.1016/j.epsl.2011.10.008

Bolhar, R., and Van Kranendonk, M. J. (2007). A non-marine depositional setting for the northern Fortescue Group, Pilbara Craton, inferred from trace element geochemistry of stromatolitic carbonates. *Precambrian Res.* 155, 229–250. doi:10.1016/j.precamres.2007.02.002

Bosak, T., Knoll, A. H., and Petroff, A. P. (2013). The meaning of stromatolites. *Annu. Rev. Earth Planet. Sci.* 41, 21–44. doi:10.1146/annurev-earth-042711-105327

Burne, R. V., and Moore, L. S. (1987). Microbialites: organosedimentary deposits of benthic microbial communities. *Palaios* 2, 241–254. doi:10.2307/3514674

Burns, S. J., Mckenzie, J. A., and Vasconcelos, C. (2000). Dolomite formation and biogeochemical cycles in the Phanerozoic. *Sedimentology* 47, 49–61. doi:10.1046/j.1365-3091.2000.00004.x

Byrne, R. H., and Sholkovitz, E. R. (1996). "Chapter 158 Marine chemistry and geochemistry of the lanthanides," in *Handbook on the physics and chemistry of rare earths*. Editors K. A. Gschneidner, and L. Eyring (Amsterdam, Netherlands: Elsevier), 497–593. doi:10.1016/S0168-1273(96)23009-0

Carpenter, S. J., and Lohmann, K. C. (1992). Ratios of modern marine calcite: empirical indicators of ocean chemistry and precipitation rate. *Geochim. Cosmochim. Acta* 56, 1837–1849. doi:10.1016/0016-7037(92)90314-9

Chang, B., Li, C., Liu, D., Foster, I., Tripati, A., Lloyd, M. K., et al. (2020). Massive formation of early diagenetic dolomite in the Ediacaran Ocean: constraints on the "dolomite problem.". *Proc. Natl. Acad. Sci. U. S. A.* 117, 14005–14014. doi:10.1073/pnas.1916673117

Chen, X., Xu, Q., Hao, F., Chen, Y., Yi, Y., Hu, F., et al. (2023). Dolomite reservoir formation and diagenesis evolution of the upper ediacaran Qigebrak Formation in the tabei area, Tarim Basin. *Sci. China Earth Sci.* 66, 2311–2331. doi:10.1007/s11430-022-1103-4

Chen, Y., Shen, A., Pan, L., Zhang, J., and Wang, X. (2017). Features, origin and distribution of microbial dolomite reservoirs: a case study of 4th Member of Sinian Dengying Formation in Sichuan Basin, SW China. *Petrol. explor. Dev.* 44, 745–757. doi:10.1016/S1876-3804(17)30085-X

Cui, H., Xiao, S., Cai, Y., Peek, S., Plummer, R. E., and Kaufman, A. J. (2019). Sedimentology and chemostratigraphy of the terminal ediacaran Dengying Formation at the gaojiashan section, south China. *Geol. Mag.* 156, 1924–1948. doi:10.1017/S0016756819000293

Deng, B., Wu, J., Li, W., Lu, P., Tian, T., Jiang, H., et al. (2022). U-Pb dating and trapped hydrocarbon inclusions in carbonate for petroleum accumulation: case study from the Sinian Dengying Formation in the central Sichuan Basin. *Nat. Gas. Geosci.* 34, 1–15. doi:10.11764/j.issn.1672-1926.2023.07.007

Ding, Y., Chen, D., Zhou, X., Guo, C., Huang, T., and Zhang, G. (2019). Cavity-filling dolomite speleothems and submarine cements in the Ediacaran Dengying microbialites, South China: responses to high-frequency sea-level fluctuations in an aragonite-dolomite sea. *Sedimentology* 66, 2511–2537. doi:10.1111/sed.12605

Dupraz, C., and Visscher, P. T. (2005). Microbial lithification in marine stromatolites and hypersaline mats. *Trends Microbiol.* 13, 429–438. doi:10.1016/j.tim.2005.07.008

Fairchild, I. J., and Spiro, B. (1987). Petrological and isotopic implications of some contrasting Late Precambrian carbonates, NE Spitsbergen. *Sedimentology* 34, 973–989. doi:10.1111/j.1365-3091.1987.tb00587.x

Feng, M., Wu, P., Qiang, Z., Liu, X., Duan, Y., and Xia, M. (2017). Hydrothermal dolomite reservoir in the precambrian Dengying Formation of central Sichuan Basin, southwestern China. *Mar. Pet. Geol.* 82, 206–219. doi:10.1016/j.marpetgeo.2017.02.008

Grey, K., and Awramik, S. M. (2020). *Handbook for the study and description of microbialites*. Perth: Geological Survey of.

Grotzinger, J., and Al-Rawahi, Z. (2014). Depositional facies and platform architecture of microbialite-dominated carbonate reservoirs, Ediacaran–Cambrian Ara Group, Sultante of Om. *AAPG Bull.* 98, 1453–1494. doi:10.1306/02271412063

Halverson, G. P., Wade, B. P., Hurtgen, M. T., and Barovich, K. M. (2010). Neoproterozoic chemostratigraphy. *Precambrian Res.* 182, 337–350. doi:10.1016/j.precamres.2010.04.007

Harwood, C. L., and Sumner, D. Y. (2012). Origins of microbial microstructures in the Neoproterozoic Beck Spring Dolomite: variations in microbial community and timing of lithification. *J. Sediment. Res.* 82, 709–722. doi:10.2110/jsr.2012.65

Harwood Theisen, C., and Sumner, D. Y. (2016). Thrombolite fabrics and origins: influences of diverse microbial and metazoan processes on Cambrian thrombolite variability in the Great Basin, California and Nevada. *Sedimentology* 63, 2217–2252. doi:10.1111/sed.12304

Hood, A. v.S., Wallace, M. W., and Drysdale, R. N. (2011). Neoproterozoic aragonite-dolomite seas? Widespread marine dolomite precipitation in Cryogenian reef complexes. *Geology* 39, 871–874. doi:10.1130/G32119.1

Huang, H., Huyskens, M. H., Yin, Q.-Z., Cawood, P. A., Hou, M., Yang, J., et al. (2022). Eruptive tempo of Emeishan large igneous province, southwestern China and northern Vietnam: relations to biotic crises and paleoclimate changes around the Guadalupian-Lopingian boundary. *Geology* 50, 1083–1087. doi:10.1130/G50183.1

Jafarian, A., Javanbakht, M., Koeshidayatullah, A., Pimentel, N., Salad Hersi, O., Yahyaei, A., et al. (2018). Paleoenvironmental, diagenetic, and eustatic controls on the permo–triassic carbonate–evaporite reservoir quality, upper dalan and kangan formations, lavan gas field, Zagros Basin. *Geol. J.* 53, 1442–1457. doi:10.1002/gj.2965

Jiang, H., Wang, Z., Du, H., Zhang, C., Wang, R., Zou, N., et al. (2014). Tectonic evolution of the Leshan-Longnvsi paleo-uplift and peservoir pormation of Neoproterozoic Sinian gas. *Nat. Gas. Geosci.* 25, 192–200. doi:10.11764/j.issn.1672-1926.2014.02.192

Jin, M., Li, B., Zhu, X., Dai, L., Jiang, Z., Wu, H., et al. (2020). Characteristics and main controlling factors of reservoirs in the fourth member of Sinian Dengying Formation in Yuanba and its peripheral area, northeastern Sichuan Basin, SW China. *Petrol. explor. Dev.* 47, 1172–1182. doi:10.1016/S1876-3804(20)60127-1

Katz, D. A., Eberli, G. P., Swart, P. K., and Smith, L. B. (2006). Tectonic-hydrothermal brecciation associated with calcite precipitation and permeability destruction in Mississippian carbonate reservoirs, Montana and Wyoming. *AAPG Bull.* 90, 1803–1841. doi:10.1306/03200605072

Kennard, J. M. (1994). "Thrombolites and stromatolites within shale-carbonate cycles, middle-late cambrian shannon formation, amadeus basin, Central Australia," in *Phanerozoic stromatolites II*. Editors J. Bertrand-Sarfati, and C. Monty (Dordrecht: Springer Netherlands), 443–471. doi:10.1007/978-94-011-1124-9_17

Kennard, J. M., and James, N. P. (1986). Thrombolites and stromatolites: two distinct types of microbial structures. *Palaios* 1, 492–503. doi:10.2307/3514631

Land, L. S. (1985). The origin of massive dolomite. *J. Geol. Educ.* 33, 112–125. doi:10.5408/0022-1368-33.2.112

Li, Y., Liu, G., Song, Z., Sun, M., Tian, X., Yang, D., et al. (2023a). Constraints of C-O-Sr isotope and elemental geochemistry on the origin of dolomite of the deeply buried Ediacaran sedimentary succession, central Sichuan Basin (SW China). *J. Asian Earth Sci.* 255, 105780. doi:10.1016/j.jseaes.2023.105780

Li, Y., Wu, B., Zhang, J., Liu, X., Xie, G., Jiang, Q., et al. (2023b). Effect of pyrobitumen on the carbonate reservoir performance. *Carbonates Evaporites* 38, 25. doi:10.1007/s13146-023-00847-z

Liu, S., Yang, Y., Deng, B., Zhong, Y., Wen, L., Sun, W., et al. (2021). Tectonic evolution of the Sichuan Basin, southwest China. *Earth-Sci. Rev.* 213, 103470. doi:10.1016/j.earscirev.2020.103470

Longman, M. W. (1980). Carbonate diagenetic textures from nearsurface diagenetic environments. *AAPG Bull.* 64, 461–487. doi:10.1306/2F918A63-16CE-11D7-8645000102C1865D

Lu, P., Li, Z., Tian, T., Wu, J., Sun, W., and Qiao, Z. (2023). The botryoidal-lace texture and its role in dolomite reservoir control in the 2nd Member, Sinian Dengying Formation in Sichuan Basin. *Earth Sci. Front.* 30, 14–31. doi:10.13745/j.esf.sf.2023.2.15

Lukoczki, G., Haas, J., Gregg, J. M., Machel, H. G., Kele, S., and John, C. M. (2020). Early dolomitization and partial burial recrystallization: a case study of Middle Triassic peritidal dolomites in the Villány Hills (SW Hungary) using petrography, carbon, oxygen, strontium and clumped isotope data. *Int. J. Earth Sci.* 109, 1051–1070. doi:10.1007/s00531-020-01851-7

Mancini, E. A., Llinás, J. C., Parcell, W. C., Aurell, M., Bádenas, B., Leinfelder, R. R., et al. (2004). Upper Jurassic thrombolite reservoir play, northeastern Gulf of Mexico. *AAPG Bull.* 88, 1573–1602. doi:10.1306/06210404017

Mancini, E. A., Parcell, W. C., and Ahr, W. M. (2006). Upper Jurassic Smackover thrombolite buildups and associated nearshore facies, southwest Alabama. *Gulf Coast Assoc. Geol. Soc. Trans.* 56, 551–563.

Mather, C. C., Lampinen, H. M., Tucker, M., Leopold, M., Dogramaci, S., Raven, M., et al. (2023). Microbial influence on dolomite and authigenic clay mineralisation in dolocrete profiles of NW Australia. *Geobiology* 21, 644–670. doi:10.1111/gbi.12555

May, W. E., Parris, R. M., Ii, C. M. B., Fassett, J. D., Greenberg, R. R., Guenther, F. R., et al. (2000). "Definitions of terms and modes used at NIST for value-assignment of reference materials for chemical measurement," in *Reference materials in analytical chemistry: a guide for selection and use*. Editor A. Zschunke (Berlin: Springer Verlag GmbH and Co.), 34–50.

McLennan, S. M. (1989). Rare earth elements in sedimentary rocks; influence of provenance and sedimentary processes. *Rev. Mineral. Geochem.* 21, 169–200.

Moore, L. S., and Burne, R. V. (1994). in *The modern thrombolites of Lake Clifton, western Australia*. Editors I. I. Phanerozoic stromatolites, J. Bertrand-Sarfati, and C. Monty (Dordrecht: Springer Netherlands), 3–29. doi:10.1007/978-94-011-1124-9_1

Murray, S. T., Higgins, J. A., Holmden, C., Lu, C., and Swart, P. K. (2021). Geochemical fingerprints of dolomitization in Bahamian carbonates: evidence from sulphur, calcium, magnesium and clumped isotopes. *Sedimentology* 68, 1–29. doi:10.1111/sed.12775

Nelson, W. A., and Read, J. F. (1990). Updip to downdip cementation and dolomitization patterns in a Mississippian aquifer, Appalachians. *J. Sediment. Res.* 60, 379–396. doi:10.1306/212F91A1-2B24-11D7-8648000102C1865D

Peng, B., Li, Z., Li, G., Liu, C., Zhu, S., Zhang, W., et al. (2018). Multiple dolomitization and fluid flow events in the precambrian Dengying Formation of Sichuan Basin, southwestern China. *Acta Geol. Sin. Engl. Ed.* 92, 311–332. doi:10.1111/1755-6724.13507

Pratt, B. R. (1982). Stromatolite decline—a reconsideration. *Geology* 10, 512–515. doi:10.1130/0091-7613(1982)10<512:sdr>2.0.co;2

Pratt, B. R., and James, N. P. (1982). Cryptalgal-metazoan bioherms of early ordovician age in the st george Group, western newfoundland. *Sedimentology* 29, 543–569. doi:10.1111/j.1365-3091.1982.tb01733.x

Reid, R. P., Suosaari, E. P., Oehlert, A. M., Pollier, C. G. L., and Dupraz, C. (2024). Microbialite accretion and growth: lessons from Shark Bay and the Bahamas. *Annu. Rev. Mae. Sci.* 16, 487–511. doi:10.1146/annurev-marine-021423-124637

Riding, R. (1991). *Calcareous algae and stromatolites*. Berlin: Springer-Verlag Berlin Heidelberg.

Riding, R. (2000). Microbial carbonates: the geological record of calcified bacterial-algal mats and biofilms. *Sedimentology* 47, 179–214. doi:10.1046/j.1365-3091.2000.00003.x

Rosales, I., Pomar, L., and Al-Awwad, S. F. (2018). Microfacies, diagenesis and oil emplacement of the Upper Jurassic Arab-D carbonate reservoir in an oil field in central Saudi Arabia (Khurais Complex). *Mar. Petrol. Geol.* 96, 551–576. doi:10.1016/j.marpetgeo.2018.05.010

Scotese, C. R. (2009). Late Proterozoic plate tectonics and palaeogeography: a tale of two supercontinents, Rodinia and Pannotia. *Geol. Soc. Spec. Publ.* 326, 67–83. doi:10.1144/SP326.4

Shapiro, R. S. (2000). A comment on the systematic confusion of thrombolites. *Palaios* 15, 166–169. doi:10.2307/3515503

Shen, A., Hu, A., Cheng, T., Liang, F., Pan, W., Feng, Y., et al. (2019). Laser ablation *in situ* U-Pb dating and its application to diagenesis-porosity evolution of carbonate reservoirs. *Petrol. explor. Dev.* 46, 1127–1140. doi:10.1016/S1876-3804(19)60268-5

Sibley, D. F. (1991). Secular changes in the amount and texture of dolomite. *Geology* 19, 151–154. doi:10.1130/0091-7613(1991)019<0151:scitaa>2.3.co;2

Song, J., Liu, S., Li, Z., Luo, P., Yang, D., Sun, W., et al. (2017). Characteristics and controlling factors of microbial carbonate reservoirs in the upper sinian dengying Formation in the Sichuan Basin, China. *Oil Gas. Geol.* 38, 741–752. doi:10.11743/ogg20170411

Suarez-Gonzalez, P., Arenas, C., Benito, M. I., and Pomar, L. (2019b). Interplay between biotic and environmental conditions in pre-salt Messinian microbialites of the western Mediterranean (Upper Miocene, Mallorca, Spain). *Palaeogeogr. Palaeoclimatol. Palaeoecol.* 533, 109242. doi:10.1016/j.palaeo.2019.109242

Suarez-Gonzalez, P., Benito, M. I., Quijada, I. E., Mas, R., and Campos-Soto, S. (2019a). "Trapping and binding": a review of the factors controlling the development of fossil agglutinated microbialites and their distribution in space and time. *Earth-Sci. Rev.* 194, 182–215. doi:10.1016/j.earscirev.2019.05.007

Tahata, M., Ueno, Y., Ishikawa, T., Sawaki, Y., Murakami, K., Han, J., et al. (2013). Carbon and oxygen isotope chemostratigraphies of the Yangtze platform, South China: decoding temperature and environmental changes through the Ediacaran. *Gondwana Res.* 23, 333–353. doi:10.1016/j.gr.2012.04.005

Tang, D., Shi, X., Jiang, G., Pei, Y., Zhang, W., Wang, Y., et al. (2013). Environment controls on Mesoproterozoic thrombolite morphogenesis: a case study from the North China Platform. *J. Palaeogeogr.* 2, 275–296. doi:10.3724/SP.J.1261.2013.00031

Thompson, A., and Taylor, B. N. (2008). *Guide for the use of the international system of units (SI)*. Gaithersburg: National Institute of Standards and Technology.

Vasconcelos, C., McKenzie, J. A., Warthmann, R., and Bernasconi, S. M. (2005). Calibration of the $\delta^{18}O$ paleothermometer for dolomite precipitated in microbial cultures and natural environments. *Geology* 33, 317–320. doi:10.1130/G20992.1

Wan, T. (2012). "Tectonics of middle cambrian-early devonian the qilian tectonic period, 513–397 ma," in *The tectonics of China: data, maps and evolution*. Editor T. Wan (Berlin, Heidelberg: Springer), 87–119. doi:10.1007/978-3-642-11868-5_4

Wang, J., He, Z., Zhu, D., Liu, Q., Ding, Q., Li, S., et al. (2020a). Petrological and geochemical characteristics of the botryoidal dolomite of dengying Formation in the Yangtze Craton, south China: constraints on terminal ediacaran "dolomite seas.". *Sediment. Geol.* 406, 105722. doi:10.1016/j.sedgeo.2020.105722

Wang, L., He, Y., Peng, X., Deng, H., Liu, Y., and Xu, W. (2020b). Pore structure characteristics of an ultradeep carbonate gas reservoir and their effects on gas storage and percolation capacities in the Deng IV member, Gaoshiti-Moxi Area, Sichuan Basin, SW China. *Mar. Petrol. Geol.* 111, 44–65. doi:10.1016/j.marpetgeo.2019.08.012

Wang, L., Hu, G., Zhao, D., Tan, X., and Wang, H. (2022). Microbialites of terminal ediacaran in the upper Yangtze platform, China: from mesoscopic to nanoscale. *Palaeogeogr. Palaeoclimatol. Palaeoecol.* 585, 110729. doi:10.1016/j.palaeo.2021.110729

Wang, X., Mu, S., Fang, S., Huang, J., and Hou, F. (2000). Evolution of porosity in the process of Sinian dolostone diagenesis in southwest Sichuan. *Acta. Seismol. Sin.* 18, 549–554. doi:10.14027/j.cnki.cjxb.2000.04.012

Wen, L., Ran, Q., Tian, W., Liang, H., Zhong, Y., Zou, Y., et al. (2022). Strike-slip fault effects on diversity of the Ediacaran mound-shoal distribution in the central Sichuan Intracratonic Basin, China. *Energies* 15, 5910. doi:10.3390/en15165910

Wen, L., Zhang, J., Pan, L., Ma, H., Li, Z., Li, W., et al. (2023). Characteristics, controlling factors and exploration prospects of microbial dolomite reservoirs in the second member of Dengying Formation, Penglai-Zhongjiang area of central Sichuan Basin. *Pet. Geol. Exp.* 45, 982–993. doi:10.11781/sysydz202305982

Xia, M., Zhang, B., Jia, S., Zhao, C., Feng, M., Shang, J., et al. (2024). Retrogradation of carbonate platforms on a rifted margin: the late Ediacaran record of the northwestern Yangtze Craton (SW China). *Front. Earth Sci.* 12. doi:10.3389/feart.2024.1401426

Xu, Z., Lan, C., Zhang, B., Hao, F., Lu, C., Tian, X., et al. (2022). Impact of diagenesis on the microbial reservoirs of the terminal ediacaran Dengying Formation from the central to northern Sichuan Basin, SW China. *Mar. Petrol. Geol.* 146, 105924. doi:10.1016/j.marpetgeo.2022.105924

Yang, P., Yuan, H., Ma, K., Xiao, Q., Ye, Z., Li, Y., et al. (2023). Diagenetic fluid evolution and hydrocarbon accumulation history of second Member of the Sinian Dengying Formation in the Taihe gas area, central Sichuan basin: evidence from petrology, *in situ* geochemistry, fluid inclusions and chronology. *Acta Geol. Sin.* 97, 2332–2353. doi:10.19762/j.cnki.dizhixuebao.2023241

Yang, Y., Wang, Z., Wen, L., Xie, W., Fu, X., and Li, W. (2022). Sinian hydrocarbon accumulation conditions and exploration potential at the northwest margin of the Yangtze region, China. *Petrol. explor. Dev.* 49, 272–284. doi:10.1016/S1876-3804(22)60023-5

Yuan, H., Liu, Y., Xu, F., Wang, G., and Xu, G. (2014). The fluid charge and hydrocarbon accumulation, sinian reservoir, anpingdian-gaoshiti structure, central Sichuan Basin. *Acta Petrol. Sin.* 30, 727–736.

Yuan, Y., Shi, X., Tang, D., Shi, Q., and Li, Y. (2022). Microfabrics and organominerals as indicator of microbial dolomite in deep time: an example from the Mesoproterozoic of North China. *Precambrian Res.* 382, 106881. doi:10.1016/j.precamres.2022.106881

Zhang, J., Jones, B., Pan, L., Zhou, G., Qin, Y., Hao, Y., et al. (2014). Genesis of dolomite in the sinian dengying Formation in the Sichuan Basin. *Acta. Seismol. Sin.* 16, 715–725. doi:10.14027/j.issn.1000-0550.2018.148

Zhang, S., Jiang, G., Zhang, J., Song, B., Kennedy, M. J., and Christie-Blick, N. (2005). U-Pb sensitive high-resolution ion microprobe ages from the Doushantuo Formation in south China: constraints on late Neoproterozoic glaciations. *Geology* 33, 473–476. doi:10.1130/G21418.1

Zhao, D., Tan, X., Hu, G., Wang, L., Wang, X., Qiao, Z., et al. (2021). Characteristics and primary mineralogy of fibrous marine dolomite cements in the end-Ediacaran Dengying Formation, South China: implications for aragonite–dolomite seas. *Palaeogeogr. Palaeoclimatol. Palaeoecol.* 581, 110635. doi:10.1016/j.palaeo.2021.110635

Zhou, Y., Yang, F., Ji, Y., Zhou, X., and Zhang, C. (2020). Characteristics and controlling factors of dolomite karst reservoirs of the Sinian Dengying Formation, central Sichuan Basin, southwestern China. *Precambrian Res.* 343, 105708. doi:10.1016/j.precamres.2020.105708

Zhu, D., Liu, Q., Wang, J., Ding, Q., and He, Z. (2021). Stable carbon and oxygen isotope data of Late Ediacaran stromatolites from a hypersaline environment in the Tarim Basin (NW China) and their reservoir potential. *Facies* 67, 25. doi:10.1007/s10347-021-00633-0